united nations
educational, scientific
and cultural
organization

international atomic
energy agency

the
abdus salam
international centre for theoretical physics

SMR 1331/14

AUTUMN COLLEGE ON PLASMA PHYSICS

8 October - 2 November 2001

DYNAMIC CURRENT SHEETS

Lev Zelenyi

Russian Academy of Sciences, Space Research Institute
Moscow, Russia

INTERNATIONAL ATOMIC ENERGY AGENCY
UNITED NATIONS EDUCATIONAL, SCIENTIFIC AND CULTURAL ORGANIZATION
INTERNATIONAL CENTRE FOR THEORETICAL PHYSICS
I.C.T.P., P.O. BOX 586, 34100 TRIESTE, ITALY, CABLE: CENTRATOM TRIESTE

Lecture 1.

CURRENT SHEETS IN SPACE PLASMA

Non adiabatic particle dynamics and
numerical simulations

Lecture 2.

EQUILIBRIUM CONFIGURATIONS OF FORCED SHEETS

Role of trapped and transient populations.

Lecture 3.

FRACTAL STRUCTURES IN CURRENT SHEETS

Multiscale turbulence and current branching

Acknowledgements:

UCLA
V.Peroomian
M.Ashour-Abdalla

Maryland University
D.Schriver
M.Sitnov
S.Sharma

Calabria University
G.Zimbardo
P.Veltri
A.Greko

MPAE, Lindau
J.Büchner

Space Research Institute
A.Galeev
A.Milovanov
H.Malova
E.Grigorenko

Georgian Observatory
A.Taktakishvili

INTERNATIONAL ATOMIC ENERGY AGENCY
UNITED NATIONS EDUCATIONAL, SCIENTIFIC AND CULTURAL ORGANIZATION
INTERNATIONAL CENTRE FOR THEORETICAL PHYSICS
I.C.T.P., P.O. BOX 586, 34100 TRIESTE, ITALY, CABLE: CENTRATOM TRIESTE

Lecture 1.

CURRENT SHEETS IN SPACE PLASMA

Outline

1. **Introduction.**
   Occurrence of current sheet (CS).

2. **Models of current sheets**
   1. Isotropic models
   2. Anisotropic models (forced CS)
   3. Turbulent CS
   4. Reconnecting CS (Petchek) versus.
      Dynamic CS (Syrovatskii)

3. **Particle dynamics in CS.**
   1. Adiabaticity, Nonadiabaticity, Quasiadiabaticity.
   2. Parameters of Adiabaticity, Invariants
   3. Types of quasiadiabatic orbits.
   4. Nonadiabatic (Speiser). Particle acceleration.
   5. Formation of phase space structures.

4. **Modeling of CS formation** (Large Scale Kinetic)
   1. Shaping of magnetotail
   2. Pressure tensor and force balance

5. **Selfconsistent global kinetic models of 2D current sheets.**
   1. Model of CS population
   2. Disruptions of CS
   3. Self-adjustment of CS (overpopulation, underpopulation)
   4. Influence of electron component

6. **Conclusions:**
   Intrinsic variability of current sheets.

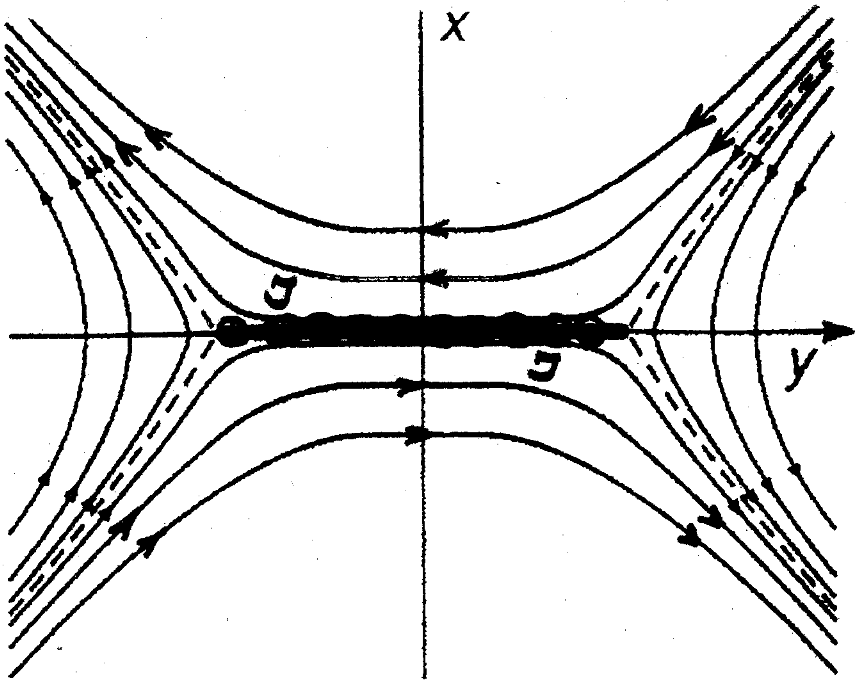

CURRENT SHEET

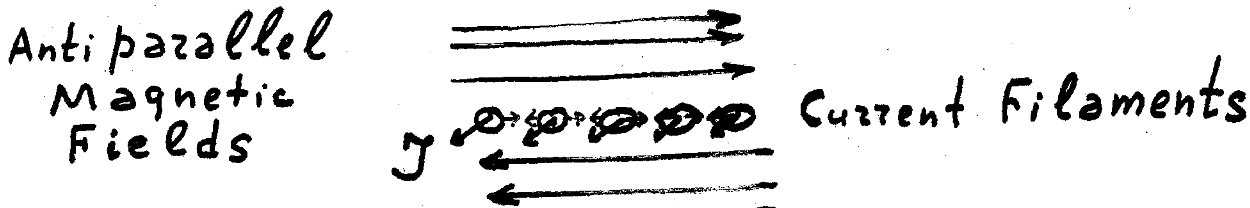

DISRUPTION OF CURRENT

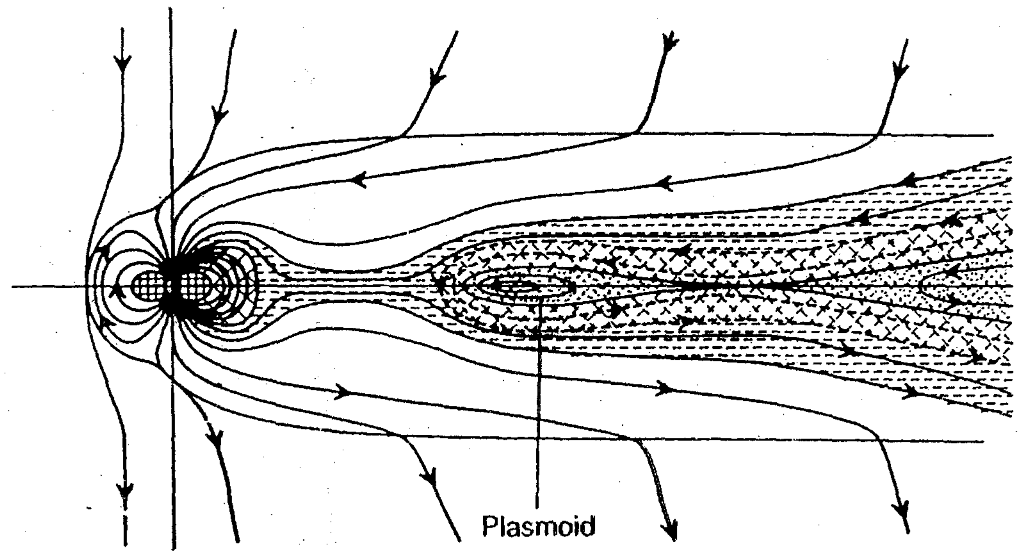

FIG. 13.23.
stage in the subs
phase, showing
moving away fr
a consequence
of the last closed
originally conne
distant neutral lir

e plasma sheet, a full-fledged substorm expansion takes place. Otherwise the disturbance is quenched, and the disturbance is called a pseu- breakup.

Once the open field lines of the tail lobe reconnect, they wrap around e plasmoid formed in the ...

SAKAI, 1996

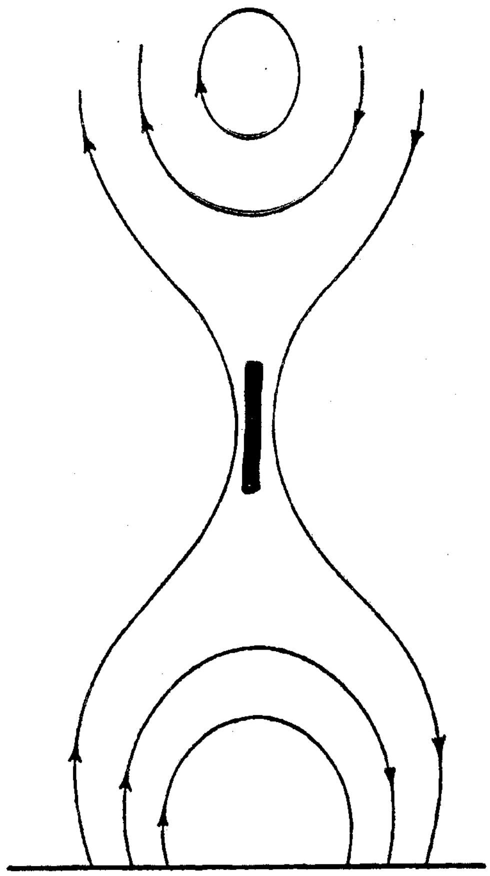

re 16. Schematic of the magnetic configuration in an eruptive/dynamic flare.

... happen at nearly the same time: The – initially open – field

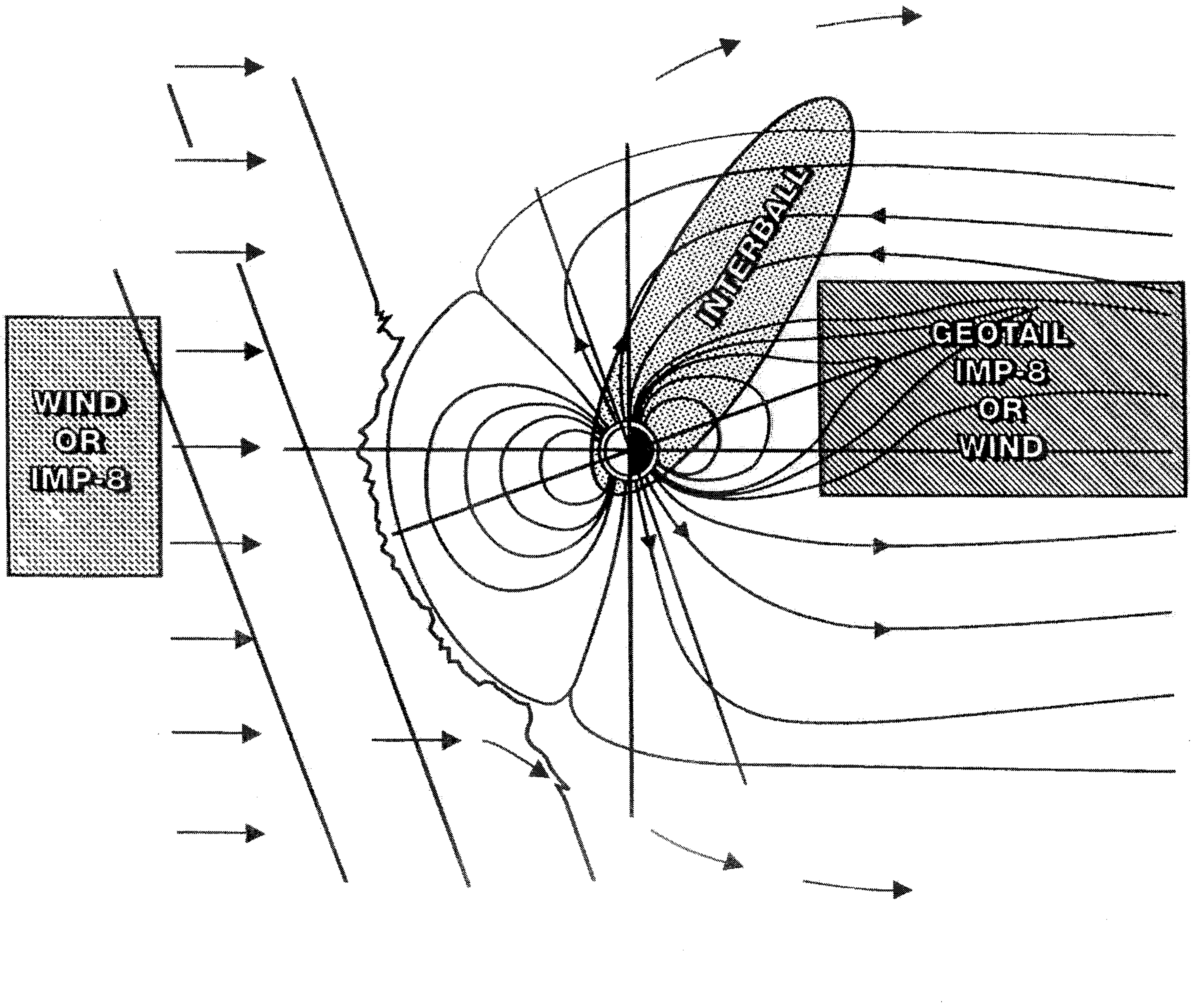
WIND
OR
IMP-8
INTERBALL
GEOTAIL
IMP-8
OR
WIND

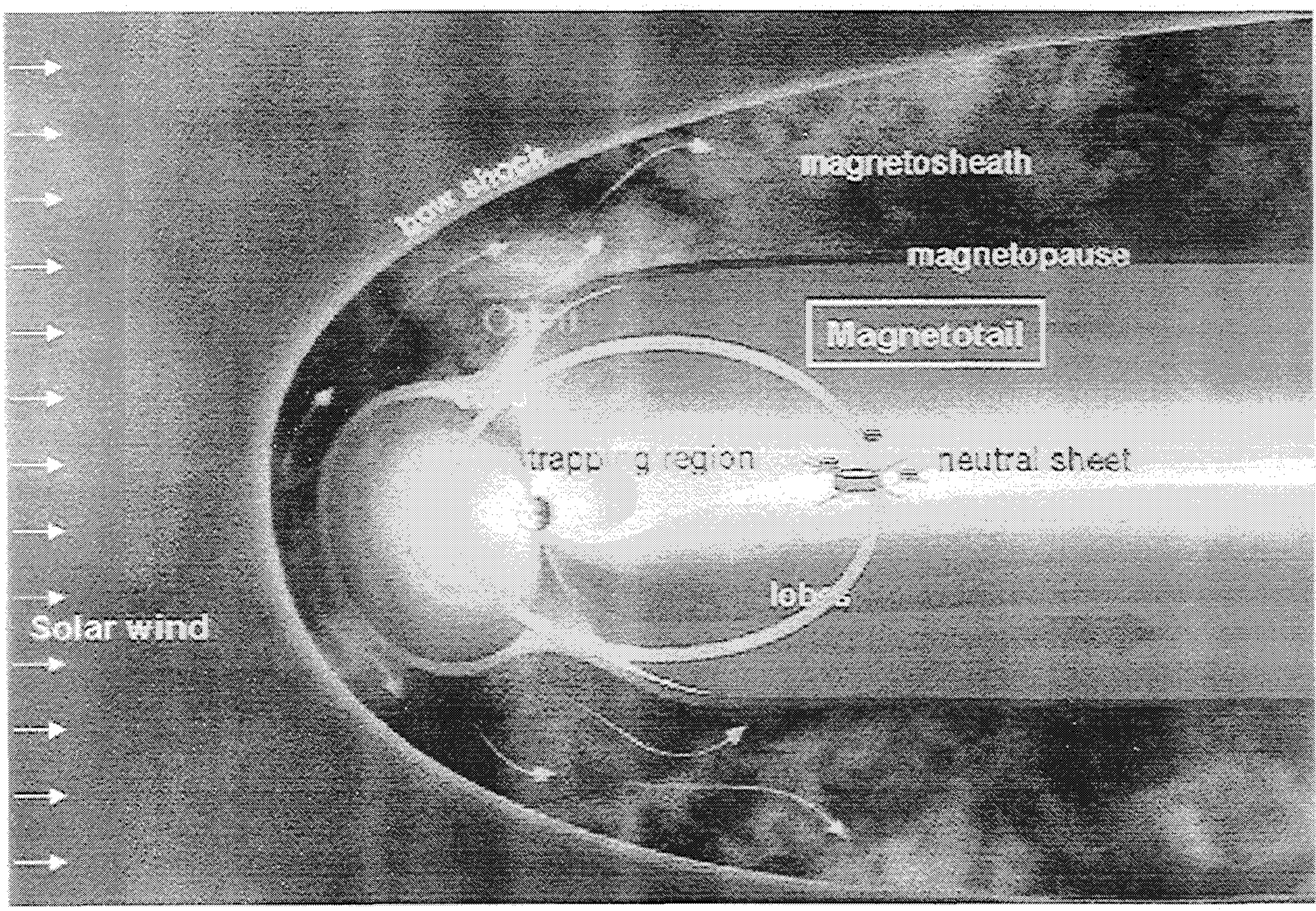
bow shock
magnetosheath
magnetopause
Magnetotail
neutral sheet
lobes
Solar wind

TSYGANENKO FIELD LINES
For IOPT=2 (Kp=1), Modified1, Modified 2
Dipole Tilt=0 Degrees

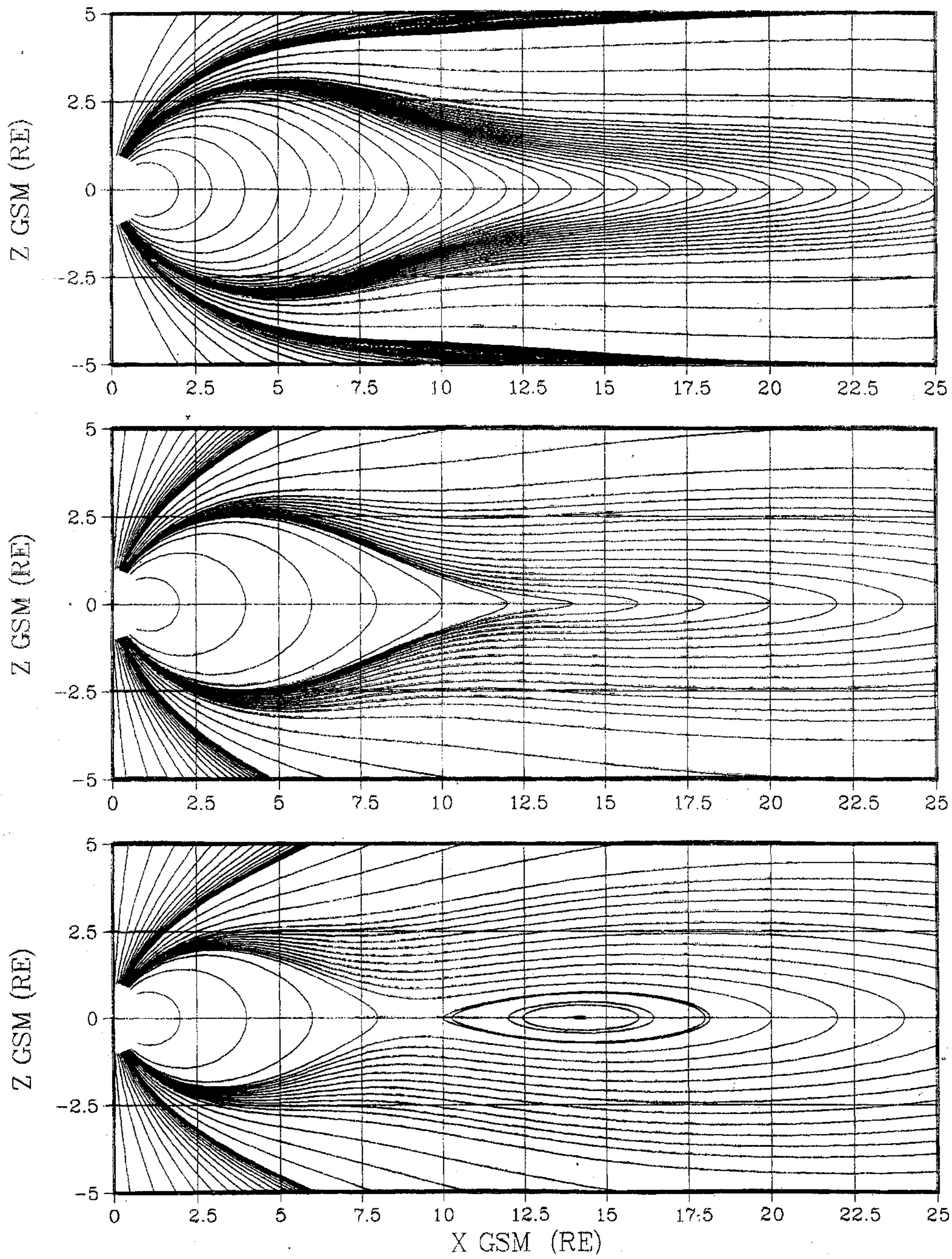

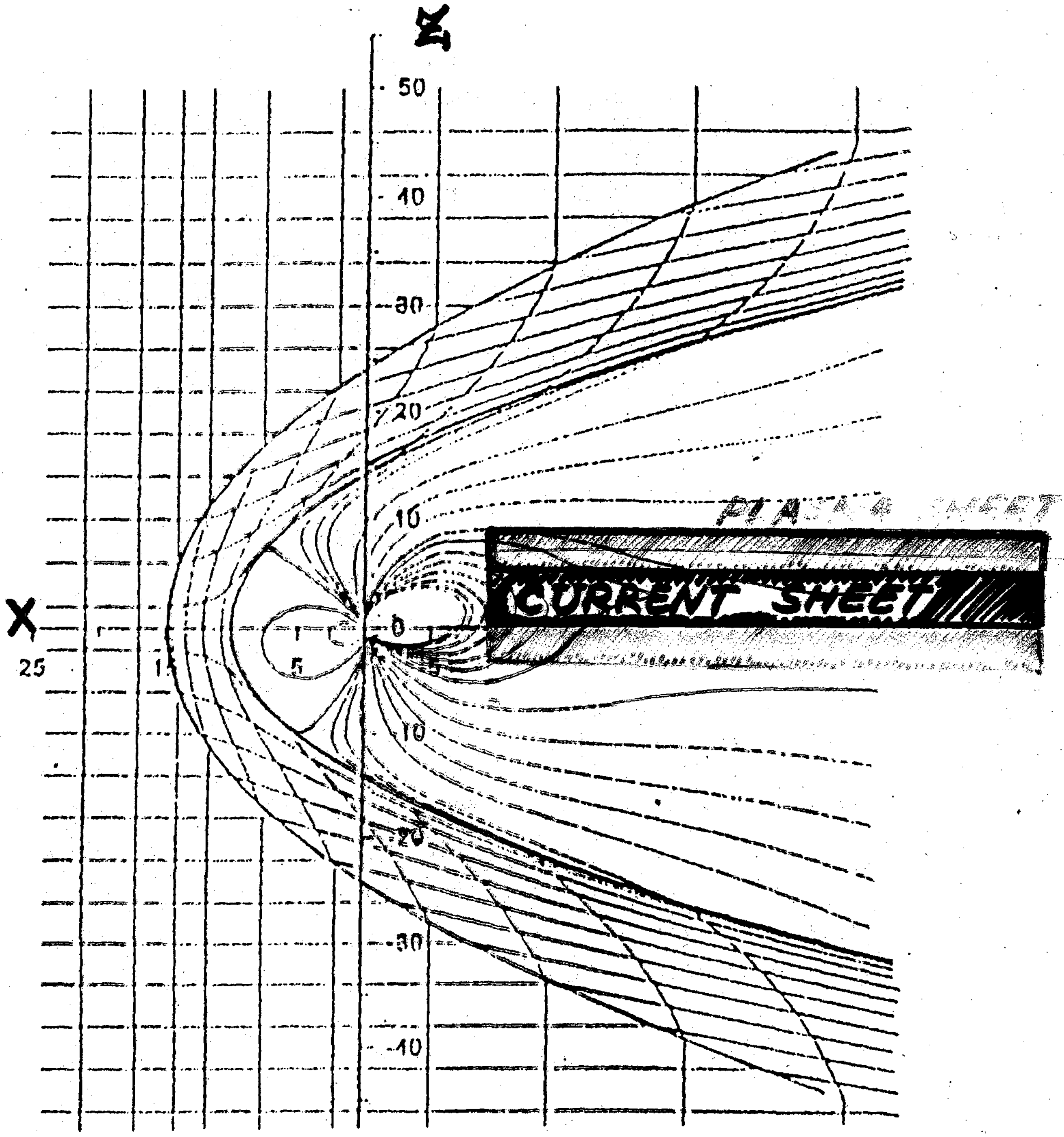
Z
50
40
30
20
10
0
10
20
30
40
X
25
5
CURRENT SHEET

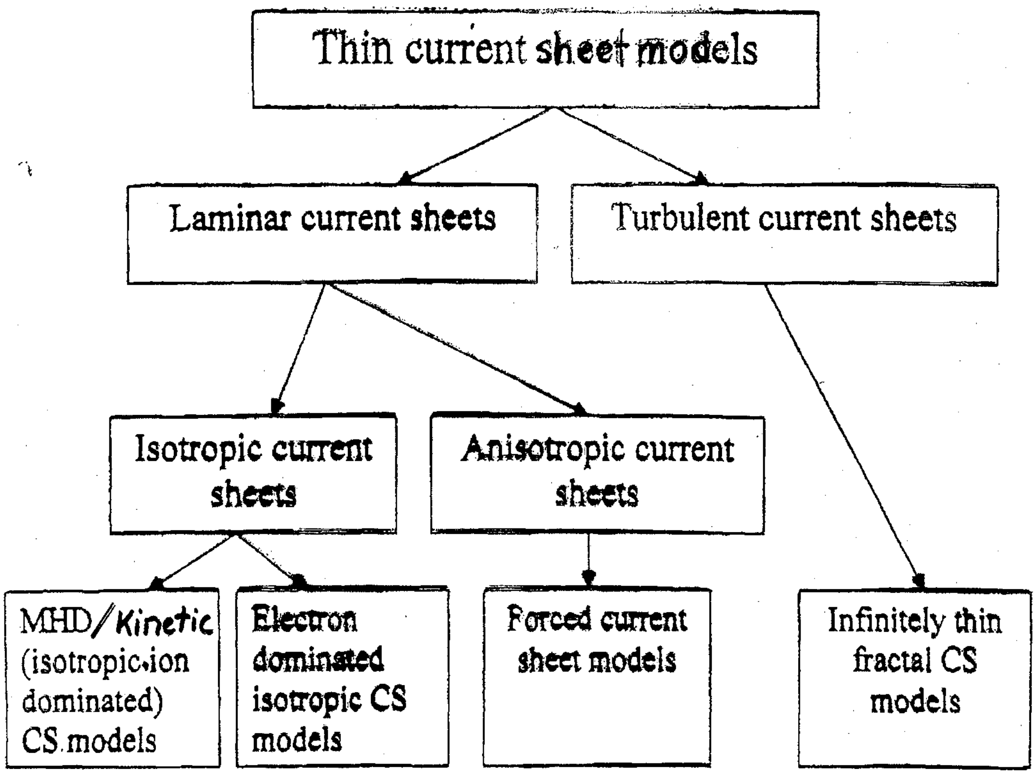

Harris [1962]
Schindler [1972]
Kan [1973]
Birn et al. [1975]
Lembege and Pellat [1982]

Schindler and Birn [1993]
Lee et al. [1995]
Wiegelmann and Schindler [1995]
Birn et al. [1998]
Schindler and Birn [1999]

Pritchett and Coroniti [1994, 1995]
Hesse and Winske [1996]
Hesse et al. [1996]
Kuznetsova et al. [1998]
Rastatter et al. [1999]
Büchner [1999]

Speiser [1970]
Eastwood [1972, 1974]
Hill [1975]
Francfort and Pellat [1976]
Burkhart et al. [1992]
Pritchett and Coroniti [1992]
Holland and Chen [1993a,b]
Ashour-Abdalla et al. [1994]
Harold and Chen [1996]
Kropotkin and Domrin [1996]
Kropotkin et al. [1997]
Sitnov et al. [1999,2000]

Milovanov et al. [1996]
Zelenyi et al. [1998]
Milovanov et al. [1999]
Veltri, [1998]
TAKTAKISHVILI, 2000, 2001

$$\frac{dN}{dt} \sim 10^{26} - 10^{27} \frac{\text{part}}{\text{sec}} \rightarrow 200 \frac{\text{gram}}{\text{sec}}$$

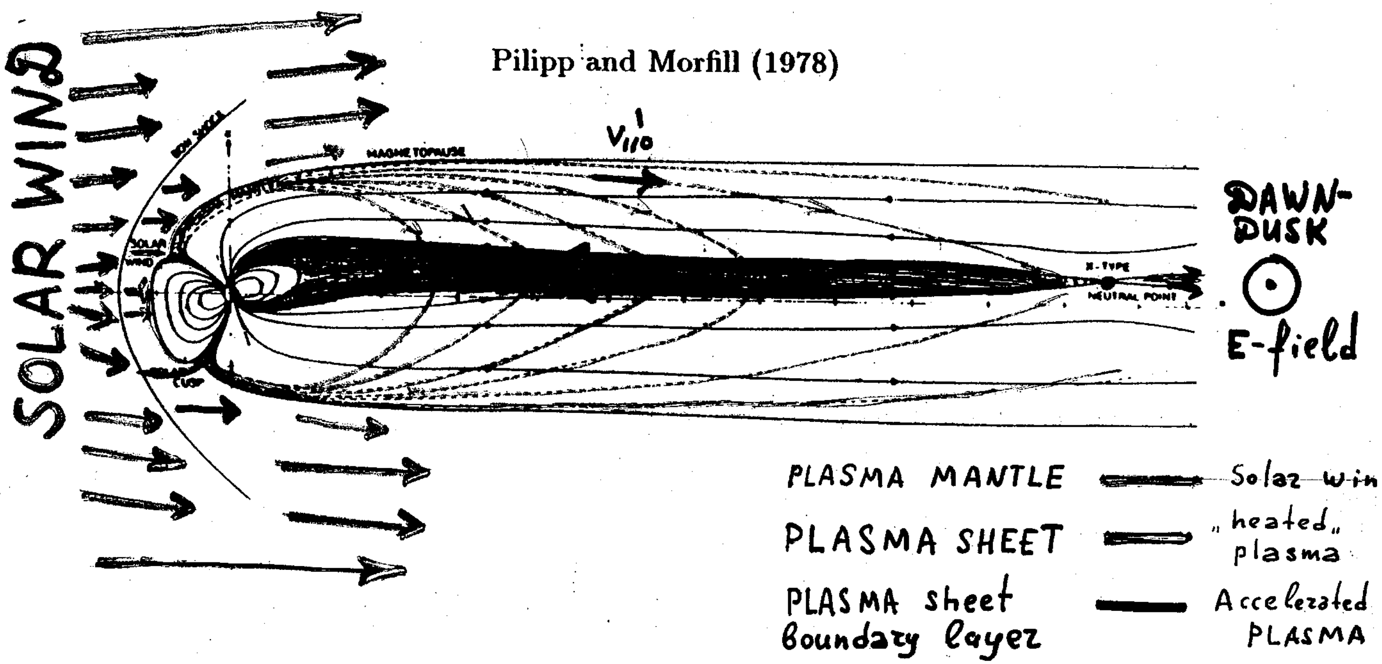

$$V_D = c\,\frac{E_y}{B_n}$$ - velocity of de Hoffman-Teller frame

$$v_{110} = V'_{110} + V_D \frac{B_0}{|\vec{B}|}$$

Harris equilibrium.

$$\boxed{f_{0j} = \frac{n_0}{ch^2(z/L)} \exp\left(\frac{m_j[(\mathrm{v}_x - V_0)^2 + (\mathrm{v}_y - u_j)^2 + \mathrm{v}_z^2]}{2T_j} \right)}$$

$$\frac{u_e}{T_e} + \frac{u_i}{T_i} = 0, \qquad L = \frac{c}{\omega_{pi}} \frac{\mathrm{v}_{Ti}}{u_i} \sqrt{\frac{T_i}{T_e + T_i}}$$

Bulk velocity (V_0) **along B does not influence** current sheet structure.

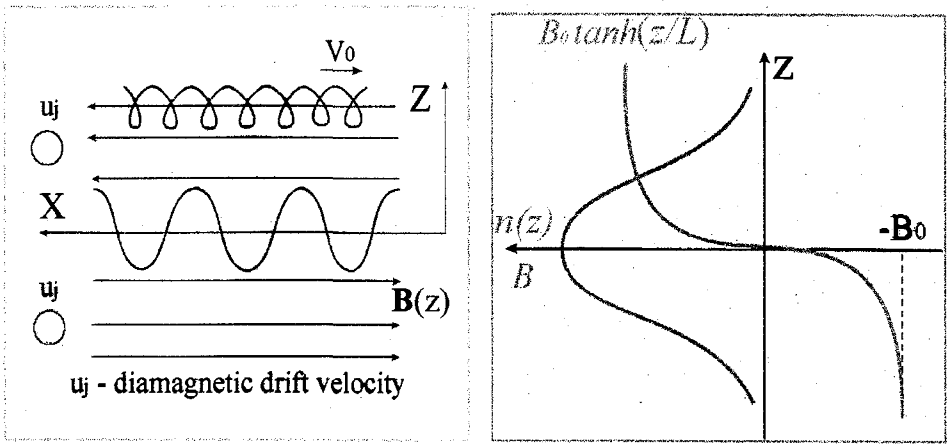

PROFILES of current and density ***COINCIDE***

$$\boxed{B_x = B_0 \tanh\left(\frac{z}{L}\right)} \quad : \quad \frac{B_0^2}{8\pi} = n_0(T_{e\perp} + T_{i\perp})$$

$$\boxed{n(z) = \frac{n_0}{ch^2\left(z/L\right)}}$$

$$J_y(z) = \sum_j e_j n_j u_j = \frac{c}{B^2}\left|\vec{B} \times \nabla p_{\perp j}\right| = \frac{J_0}{ch^2\left(z/L\right)}$$

- diamagnetic current

Forced current sheet (anisotropic) models

Main distinctive features:

- Magnetic field line tension is balanced by the ion inertia rather than by the pressure gradient; FCS resemble ED TCS with the convection field E_y having penetrated inside CS (then E_y is maybe excluded due to deHoffman-Teller system of reference)
- Current sheet thickness $L \leq \rho_{0i}$ [Franc-fort and Pellat, 1976]
- FCS provides the most natural embedding mechanism (FCS is always embedded inside the much thicker plasma sheet)

$$P_{\parallel} - P_{\perp} = \frac{B^2}{4\pi}$$

Basic FCS (quasi-adiabatic) orbits

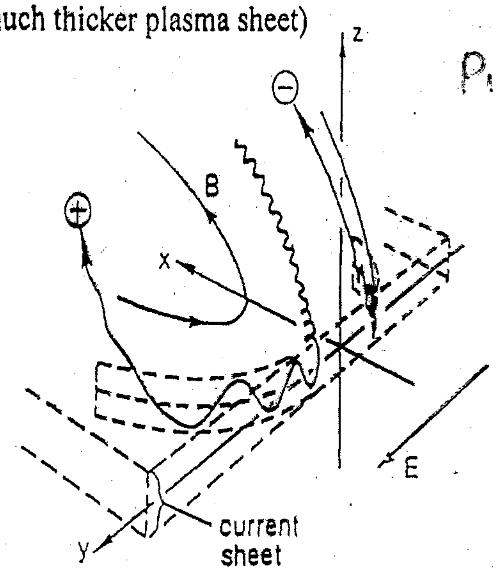

Schematic illustration of charged particle trajectories in the field reversal of Figure 3 [after *Speiser*, 1965].

Problems:

(i) numerical or non-self-consistent models;

(ii) unknown influence of electrons and electrostatic effects;

(iii) catastrophe in the limit of weak anisotropy [*Burkhart et al.*, 1992] or non-Maxwellian distribution to avoid it [*Holland and Chen*, 1993]

DUNGEY (1963)

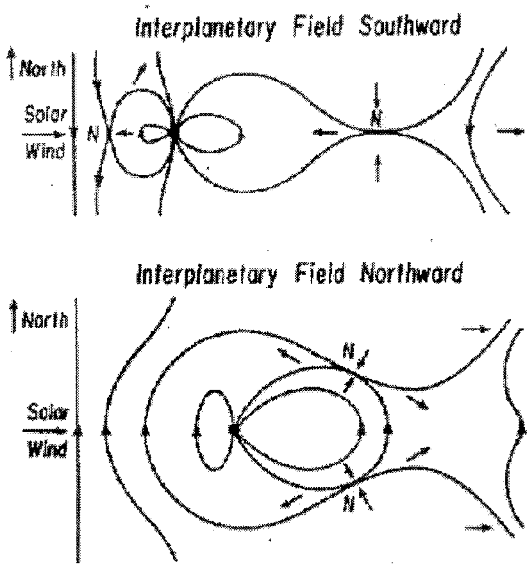

!

Reconnection

!

GLOBAL MHD

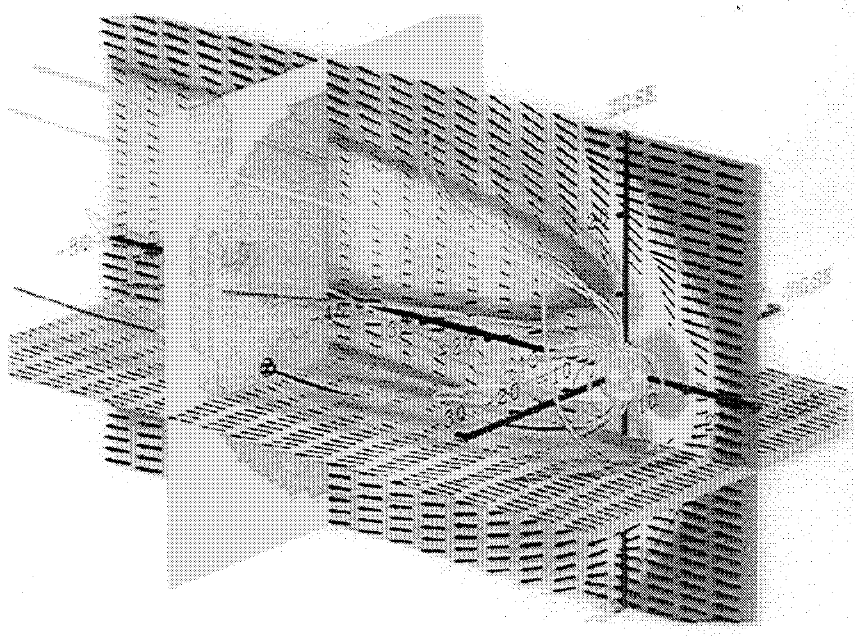

Steady Reconnection:

6.1 Current sheets: basic properties

$$\frac{u_0}{v_A} \sim \frac{\delta}{\Delta} \sim \frac{1}{\sqrt{Re_m}}$$

$$v_0 \sim v_A$$

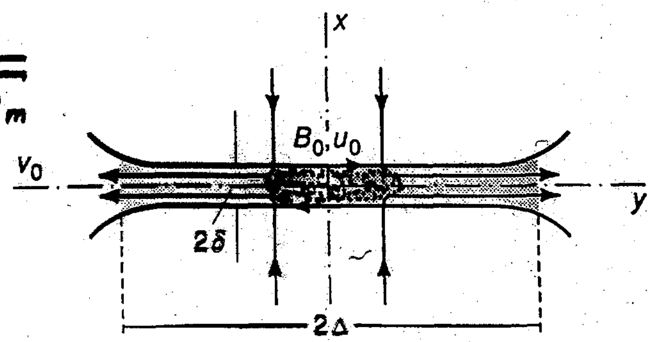

Fig. 6.2. Dynamic (Sweet-Parker) current sheet.

$$\nabla \times v_1 = \nabla \times B = 0$$

$$M = \frac{u_0}{v_A} \sim$$

$$\sim 1/\ln Re_m$$

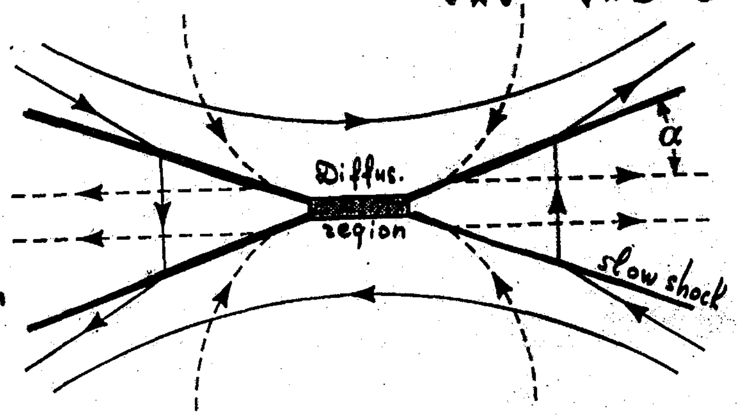

Fig. 6.3. Schematic drawing of Petschek's reconnection configuration.

Biscamp: critisism of inconsistency

Paradigm for 20 years of western hemisphere.

Generalizations of Petshek-model

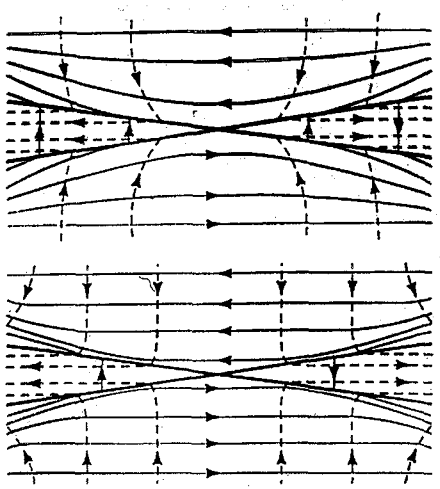

$\bar{B}_{ext} = const$

'ig. 6.5. Petschek-type reconnection configurations: magnetic field lines (full), tream lines(dashed), slow mode shocks (heavy). (a) Petschek's original config- ration ("fast mode expansion"). (b) Sonnerup-type configuration ("slow mode xpansion").

$$M = \frac{u_0}{v_A} \sim O(1)$$

P-model: Analogy with a system of two supersonic gas streams - fails

Flow is supersonic with respect to slow mode while it is Subsonic versus MAGNETOSONIC MODE

In gas - no signal could propagate upstream

In plasma - compression in front of Diff. Region is communicated upstream modifying external solution

∴ Inappropriate treatment of Diff. Region - not selfconsistent solution for η - small

Contrintuition: pushing two volumes of highly conducting plasma with $\vec{B} \downarrow\uparrow$ should produce FLATER and FLATER sheet

D. Biscamp. NL MHD, 1997

6.2.2 *Petschek's slow shock model*

The model proposed by Petschek (1964) at a symposium on solar flares was almost immediately accepted as a major breakthrough in the theory of reconnection, serving as the basic concept for the following two decades. In fact most papers (at least in the western hemisphere) on the subject of reconnection deal with one or the other variant of Petschek's model, notably the review article by Vasyliunas (1975), or a subsequent review by Forbes & Priest (1987). Only in recent years has the basic inconsistency in the theory become apparent. Because of its historical importance

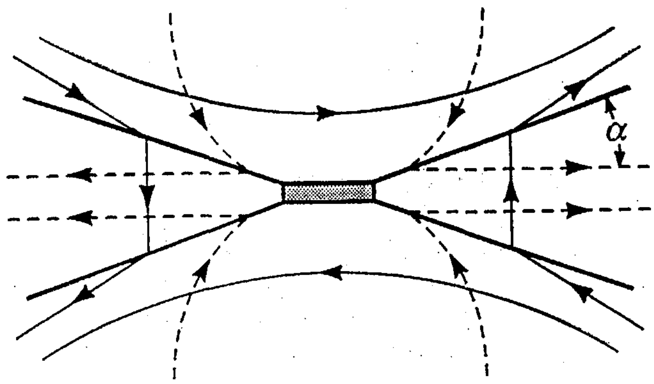

Fig. 6.3. Schematic drawing of Petschek's reconnection configuration.

Petschek's model is described briefly, before we point out where the theory is in error, both conceptually and formally.

6.2.3 *Syrovatskii's current sheet solution*

An alternative school of thought, with adherents mainly in the eastern hemisphere, originated from Syrovatskii's theory of current sheet formation (Syrovatskii, 1971). Like Petschek's model this is also a quasi-ideal, quasi-stationary approach, dealing only with the ideal solution, which may however exhibit sheet-like singularities. Though Syrovatskii's theory does not describe real configurations with high reconnection rates in the limit of small η, it provides a qualitatively correct picture for not-too-strong external driving.

Dynamic Current Sheet – Syrovatskii MODEL

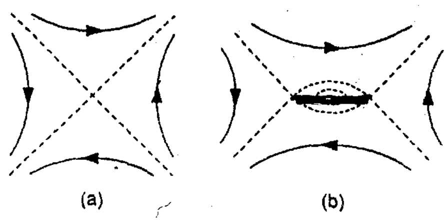

Ideal solutions with SHEET LIKE singularities

Fig. 6.6. Generation of a singular current at an X-point. (a) Initial nonsingular configuration; (b) effect of an induced singular line current in the original X-point, leading to a fictitious O-point and two adjacent X-points. The heavy line indicates the actually arising sheet current.

All currents are localized in isolated points and sheets

$$y_0^2 = \frac{I}{2\pi a} + \frac{b^2}{2}$$

$$\vec{B} = \vec{e}_z \times \nabla\psi$$

$$\boxed{\nabla^2\psi = 0}$$

ψ- harmonic function

Complex solution with BRANCH CUT = Curr. Sheet

$$I = \pi a^2 b = I_{MAX}$$

$$y_0 = b$$

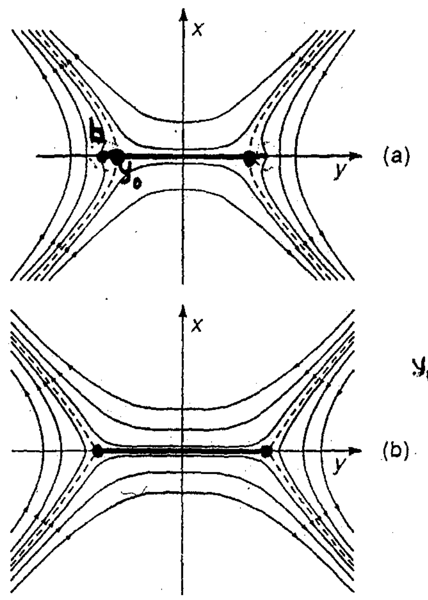

Fig. 6.7. Contours of the magnetic potential $\psi = Re\{F\}$, where F is given by eq. (6.26); heavy line = current sheet, dashed line = separatrix. (a) General case $y_0 < b$ exhibiting singularities at the current sheet endpoints; (b) limiting regular case $y_0 = b$ (from Syrovatskii, 1971).

Essential merit: simble and elegant way of generations THIN current sheets →

→ might be UNSTABLE – TEARING / sausage M.
SPONTANEOUS RECONNECTION

Syrovatskii [1971]

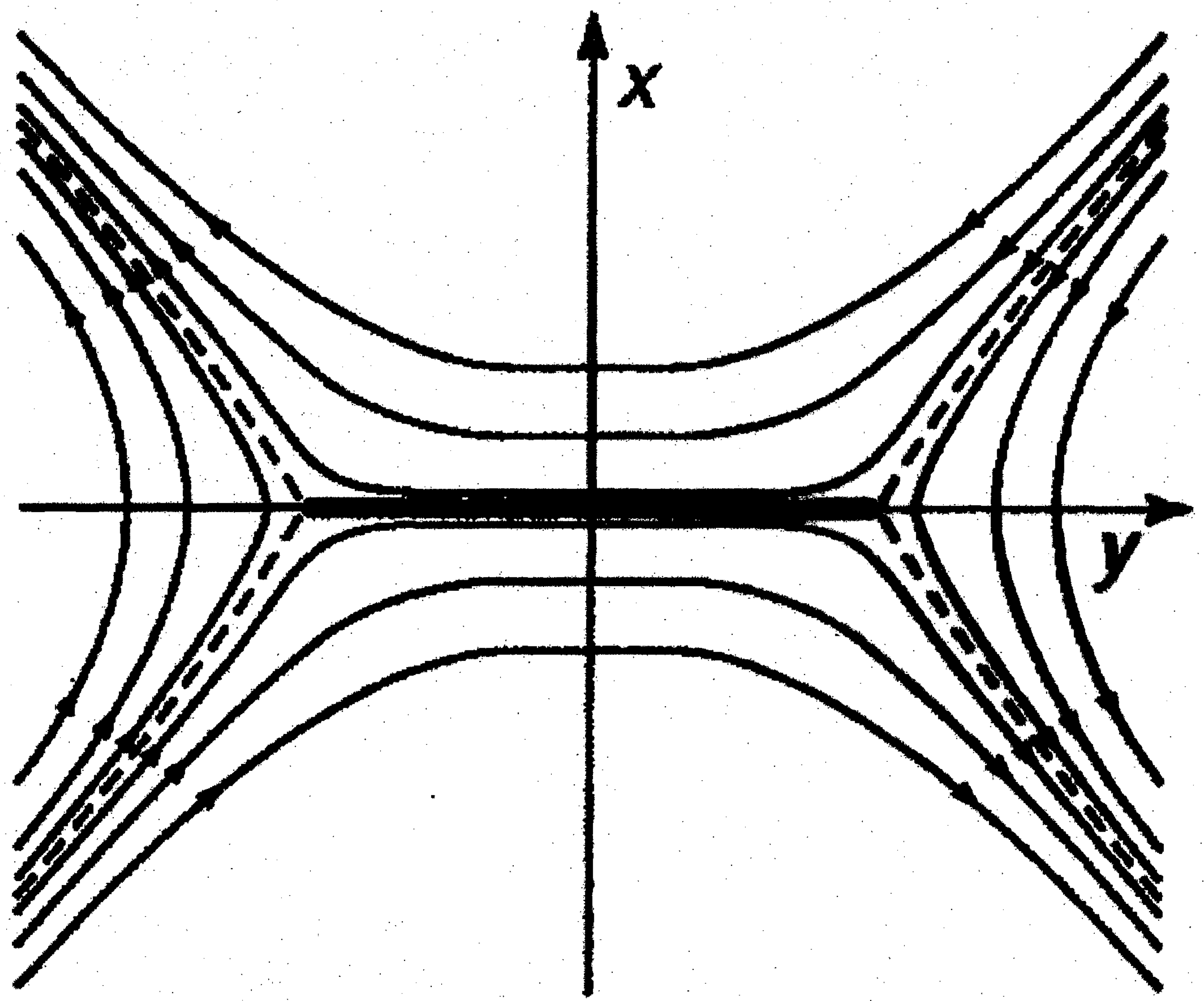

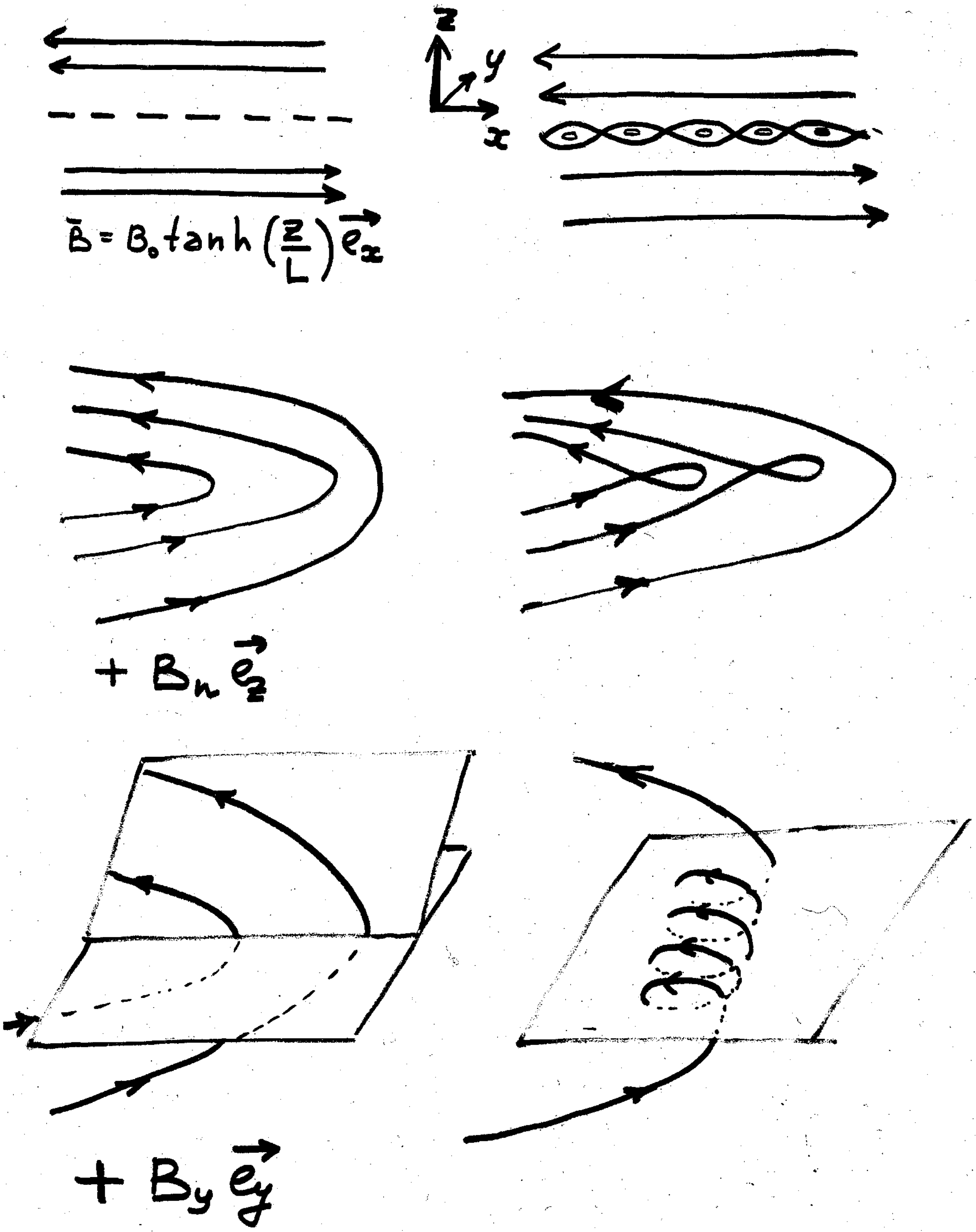
z
y
x
$\vec{B} = B_0 \tanh\left(\frac{z}{L}\right)\vec{e_x}$
$+ B_n \vec{e_z}$
$+ B_y \vec{e_y}$

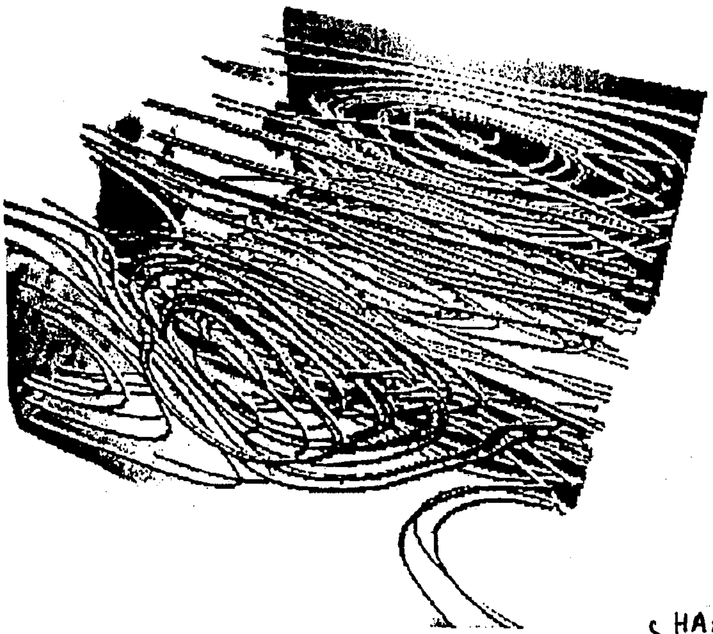

HARRIS

Fig. 3. – Magnetic field and density structure of 3D reconnection through thin current sheets.

One difference between 2D and 3D reconnection is that in three dimensions plasma outflow is possible also in the third, the original current direction.

Further, our simulations revealed regions of vanishing magnetic fields, although in their specific 3D form. Let us illustrate the generic structure of the resulting three-dimensional reconnection by showing some typical magnetic field topologies [44]. We use the results of kinetic plasma simulations with the PIC code GISMO [45]. The initial configuration is the same as for the current instability investigations before. The difference is that we now show results obtained for a mass ratio $m_e : M_i = 1 : 25$ and for an even thinner sheet, which reconnects faster.

The general picture of 3D reconnection can be seen in fig. 3. The figure combines density and magnetic field information of the developed nonlinear configurational instability in one plot. The density modulation, caused by the bulk current instability, reveals regions of enhanced and lower density. The higher density regions correspond to darker regions at the side planes of the box (in the color version on the net: blue). The side planes depict density contour plots through central cutting planes of the box in fig. 3. As one can see in the figure, and, even better, by rotating the structure using the corresponding virtual-reality-files on the net (author's homepage, click the figure), the field reminds the pattern of Petschek reconnection only near the density maxima.

FIELD REVERSAL – COUPLED OSCILLATORS

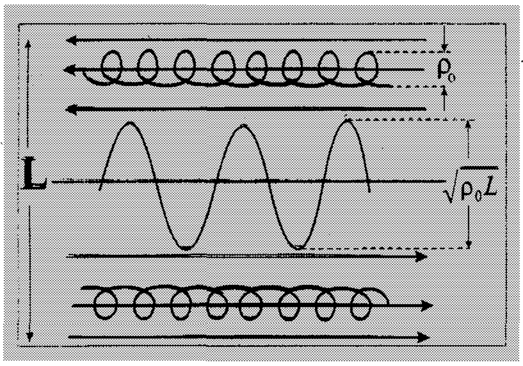

Nonlinear oscillator

$$\vec{B} = B_0 \tanh(z/L)\vec{e}_x$$

$$z \approx \operatorname{sn} \Omega_B t$$

$$\Omega_B \sim \frac{v}{d_z} \sim \frac{v}{\sqrt{\rho_0 L}}$$

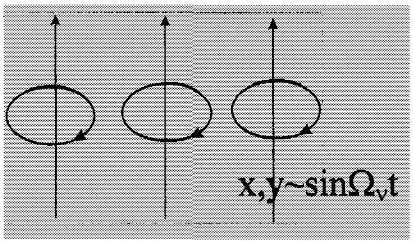

Linear oscillator

$$\vec{B} = B_n \vec{e}_z$$

$$\Omega_n = \frac{eB_n}{mc}$$

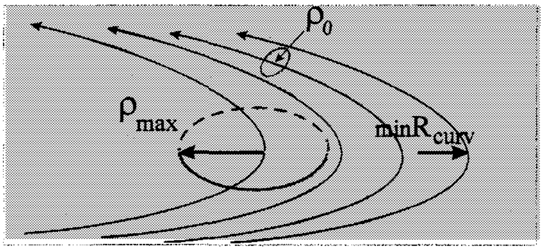

Field reversal

$$H = \underbrace{\frac{\dot{x}'^2}{2}}_{L} + \underbrace{\frac{\dot{z}^2}{2}}_{NL} + \underbrace{\frac{\kappa^2 x'^2}{2}}_{L} + \underbrace{\frac{\dot{z}^4}{8}}_{NL} - \underbrace{\frac{\kappa x' z^2}{2}}_{coupling} \equiv \frac{1}{2}$$

$$\kappa = \frac{\Omega_n}{\Omega_B} = \frac{B_n}{B_0}\sqrt{\frac{L}{\rho_0}} \equiv \left(\frac{R_{curv}^{\min}}{\rho_{\max}}\right)^{1/2}, \; x' = x - \dot{y}_0/\kappa$$

$\kappa < 1$ $z \to$ (NL) – oscillations are **FAST**

$x \to$ (L) – motion is **SLOW**

$$H = \frac{\dot{x}'^2}{2} + \frac{\dot{z}^2}{2} + \underbrace{\frac{1}{2}\left(\kappa x - \frac{z^2}{2}\right)^2}_{U(x,z)}$$

FAST OSCILLATIONS

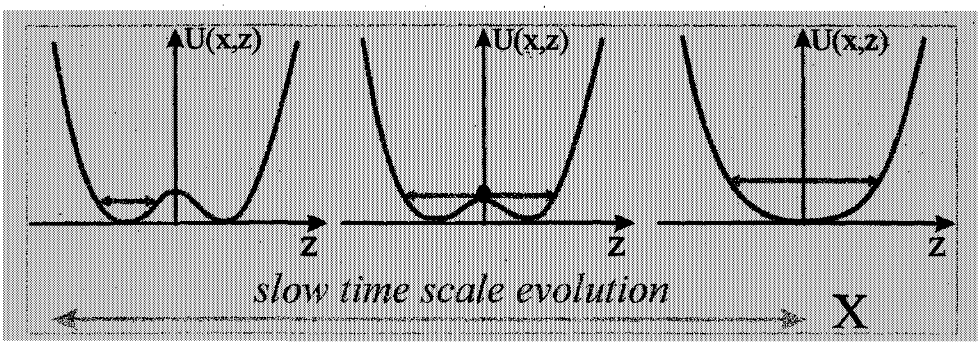

Action integral

$$I_z \equiv \frac{1}{2\pi}\oint mv_z dz \approx const$$

• - bifurcation of trajectory≡crossing of separatrix⇒ JUMPS of I_z

$$I_z = \frac{8}{3\pi}\left(\frac{\sqrt{m_i}L}{\Omega_0}\right)^{1/2}(2W)^{3/4}\cdot I'$$

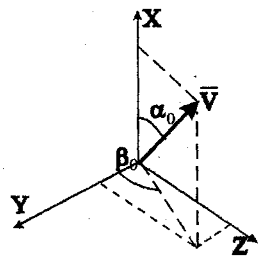

$$I' = \sin^{3/2}\alpha_0 f(k), \qquad k = \sin\frac{\beta_0}{2}$$

$$f(k) = (1-k^2)K(k) + (2k^2-1)E(k)$$

Drift-free configuration $\vec{B} = B_0 \frac{z}{L}\vec{e}_x + B_n\vec{e}_z$

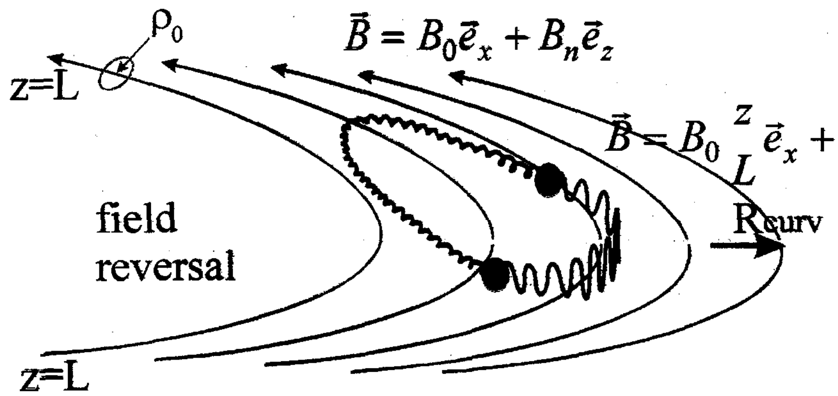

Buchner and Zelenyi, 1986,1989

$$H = \frac{\dot{x}^2}{2} + \frac{\dot{z}^2}{2} + \frac{\kappa^2 x^2}{2} + \frac{\dot{z}^4}{8} - \frac{\kappa x z^2}{2} = \frac{1}{2} \qquad x \Rightarrow x\text{-}v_y/\kappa$$

$$\kappa = \sqrt{\frac{R_{curv}^{\min}}{\rho_{\max}}} = \frac{B_n}{B_0}\sqrt{\frac{L}{\rho_0}} \sim B_n \frac{L^{1/2}}{B_0^{1/2}} W^{-1/4}$$

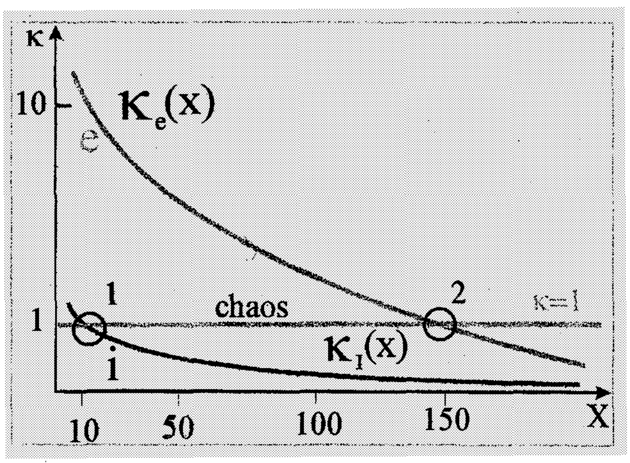

κ(x) in any realistic model

$$\kappa_i \approx \frac{\kappa_e}{10};$$

$$\left(\frac{M_i T_i}{m_e T_e}\right)^{1/4}$$

κ>1

Guiding center theory

$(v_x, v_y, v_z) \rightarrow v_\perp, v_{II}, \varphi$

Cylindrical coordinates

- $\mu = \dfrac{W_\perp}{B} = const$
- $J \equiv \dfrac{1}{2\pi}\oint v_{II} dl = const$

Double adiabatic equations: $p_\perp, p_{II}$

$$\boxed{p_{II} p_\perp^2 \sim n^5}$$

Stress-balance

$$\boxed{\rho\dot{v} = \frac{1}{c}[j \times B] - \nabla\begin{pmatrix} p_\perp & 0 & 0 \\ 0 & p_\perp & 0 \\ 0 & 0 & p_{II} \end{pmatrix}}$$

$p_{II} \rightarrow p_\perp$ due to PITCH-ANGLE DIFFUSION

gyrotropic but anisotropic $\hat{p}$

κ<1

Magnetic <u>field do not directly control</u> particle motion

$(v_x, v_y, v_z) \rightarrow (v_0, \alpha_0, \beta_0)$

Spherical coordinates

- $I_z \equiv \dfrac{1}{2\pi}\oint p_z dz$ (Speiser, 1965)
- $I_x \equiv \dfrac{1}{2\pi}\oint p_x dz$

(Zelenyi et al., 90,99)

Equation of state

$$\boxed{\frac{p^{2+\alpha} B^{2(\alpha-1)}}{n^{2+3\alpha}} = const}$$

Stress-balance

$$\boxed{\rho\dot{v} = \frac{1}{c}[j \times B] - \nabla\begin{pmatrix} p_{xx} & p_{xy} & p_{xz} \\ p_{yx} & p_{yy} & p_{yz} \\ p_{zx} & p_{zy} & p_{zz} \end{pmatrix}}$$

$$\frac{1}{c}[j \times B]_x = \frac{dp_{xz}}{dz} \quad \text{(CS)}$$

nongyrotropic $\hat{p}$

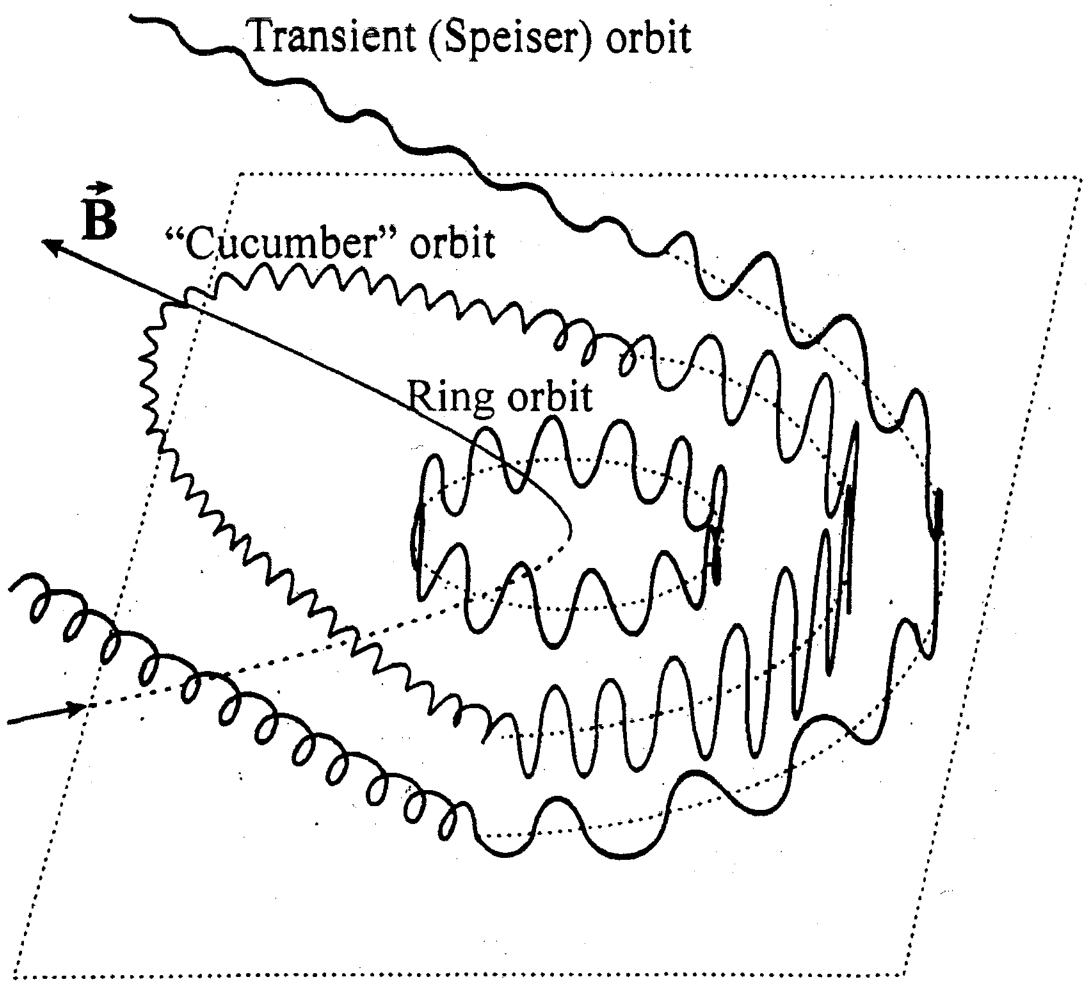

Fig. 1. Three types of particle trajectories in the magnetic field reversal. Transient (Speiser) orbits are the essential carriers of forced current sheet. "Cucumber" and ring orbits which are enclosed inside the simulation box and do not touch its boundaries are the quasi-trapped plasma.

Ashour-Abdalla, Büchner, Zelenyi, JGR

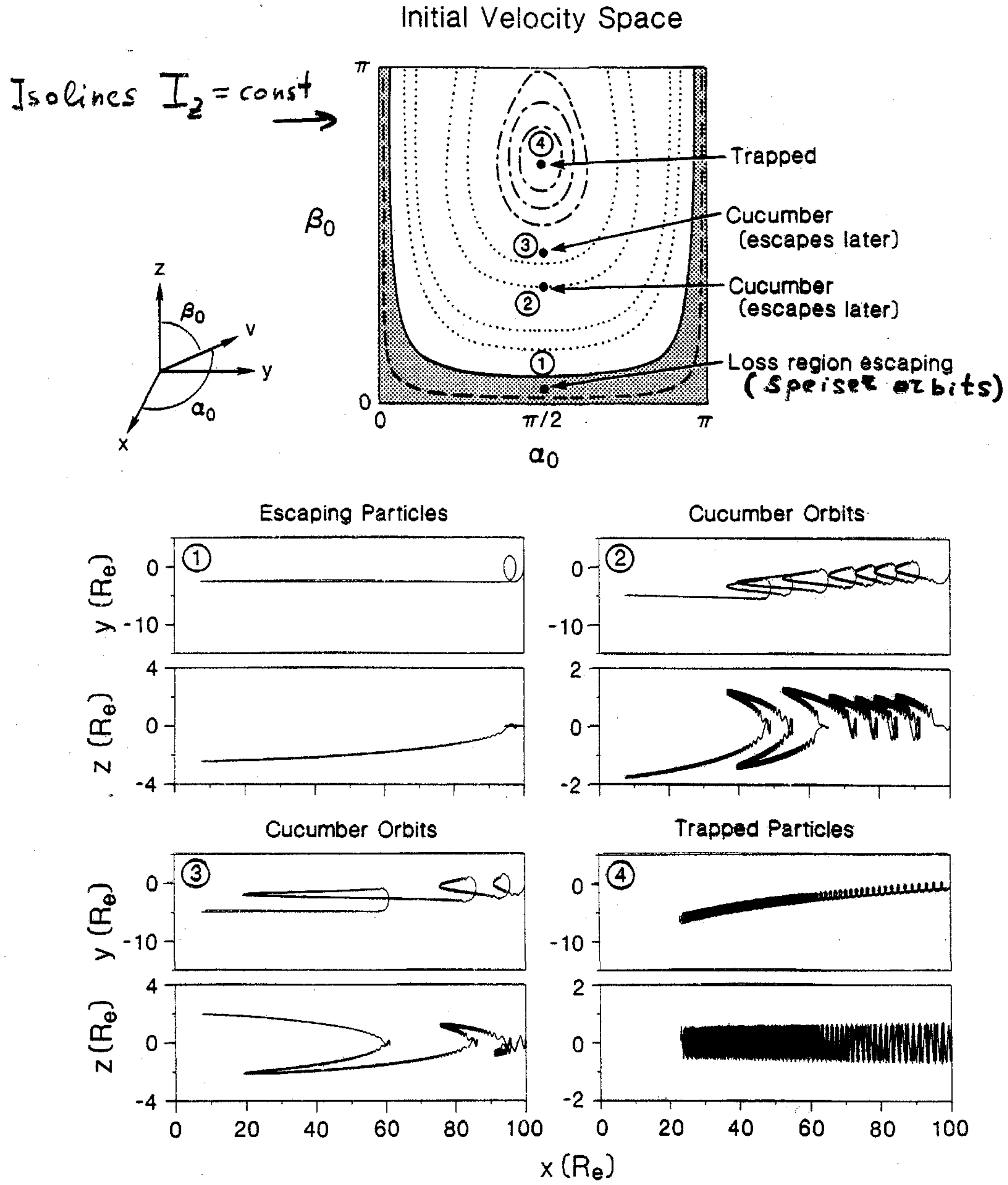

Zwingman model + dawn-dusk $\overline{E}$

$E_y \simeq 0.1$ mV/m

$$I_z \approx (W)^{3/4} f(k) = \text{const}$$

phase along orbit

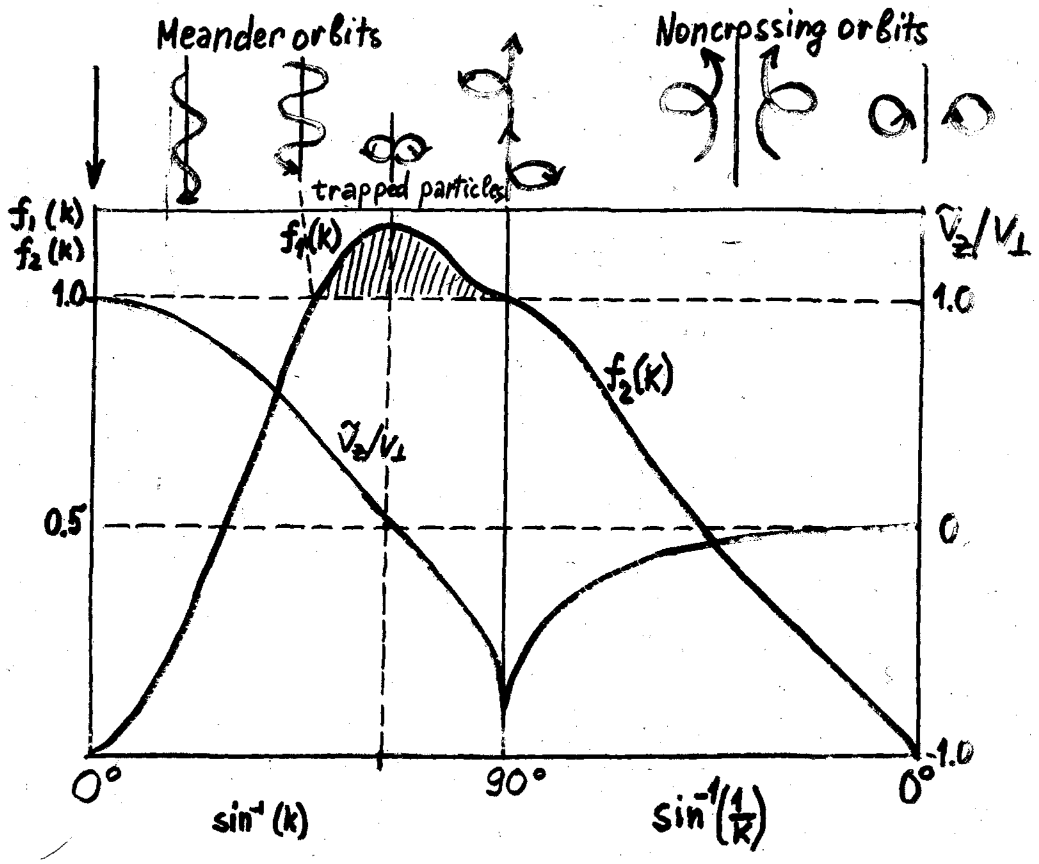

Sonnerup, 1970

The principal types of ion trajectories in TCS (X-Z plane) and corresponding current densities $j_y(Z)$

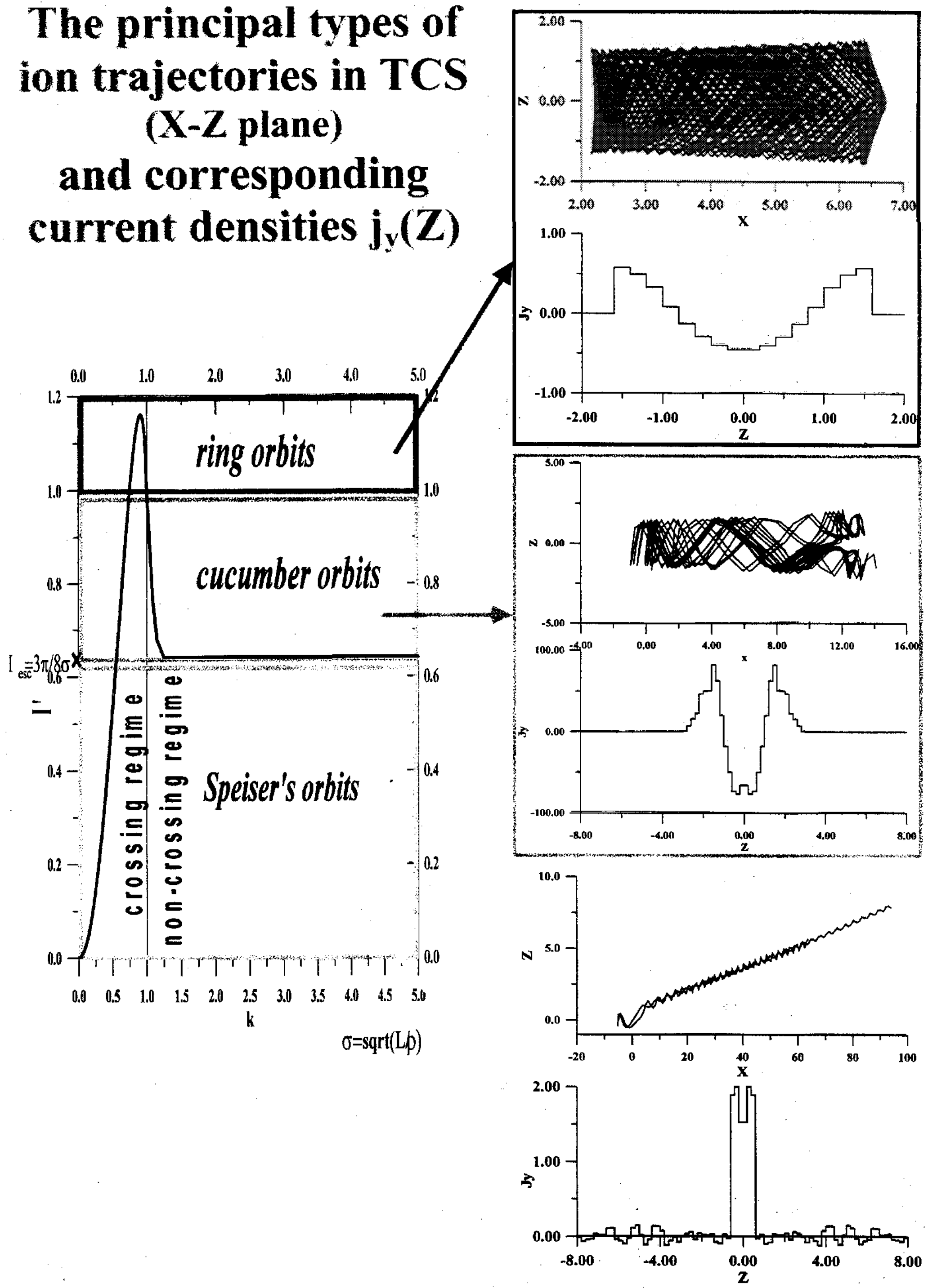

M. Ashour-Abdalla, J. Berchem; J. Buchner, L. Zelenyi — Shaping of Magnetotail — JGR april 93 — Large-scale and Small scale
- structuring → beamlets

2) Consequences of magnetotail ion dynamics JGR, october 94 → reproduces all distributions n, $\bar{v}$, • $\hat{P}_{ij}$ → pressure tensor $P_{\parallel}$, $P_{\perp}$, • P_{xz} •

- **Large-Scale Kinetics - follow trajectories of large number of non-interacting particles in specified electric and magnetic fields.**

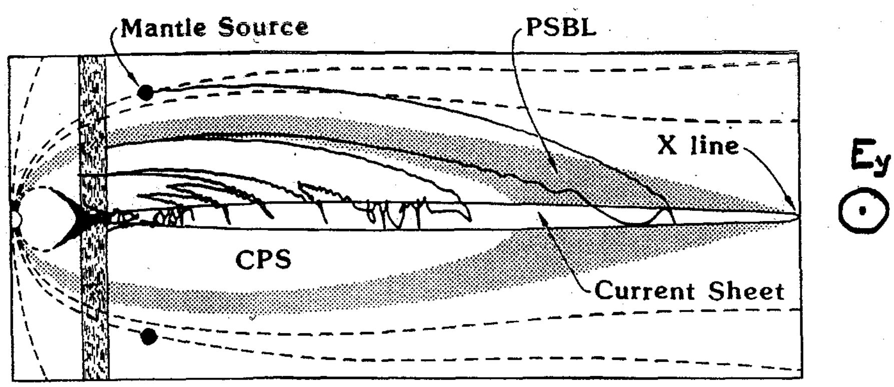

GOAL:

LSK results which include the changes in the magnetic field due to particle motion. → slow iterations

- Could we reach quasisteady convection as a balance of E_y and source intensity
- Self-adjusting topology of $\bar{B}$

?

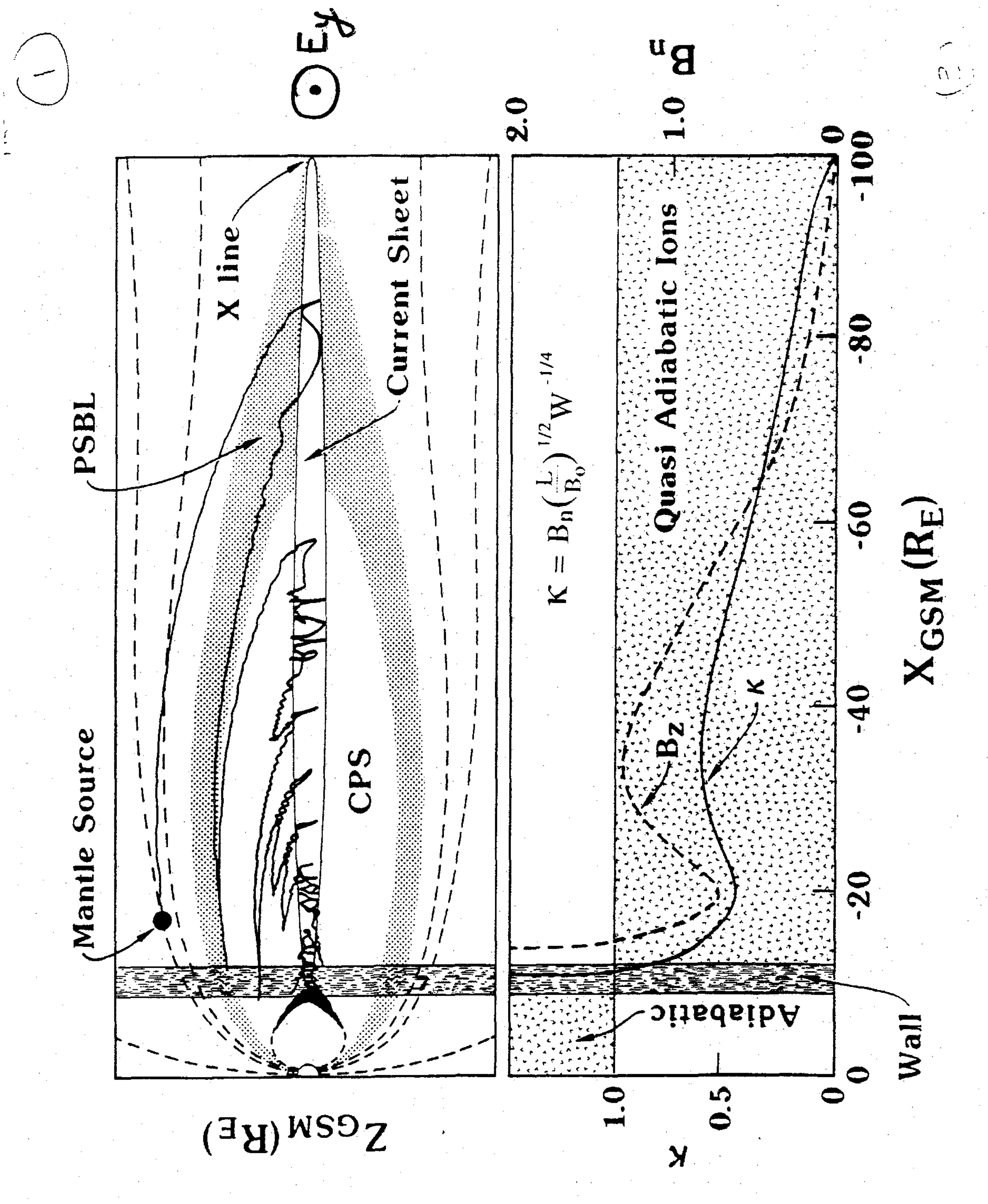

1
2
Mantle Source
PSBL
X line
Current Sheet
CPS
$\odot E_y$
$Z_{GSM}(R_E)$
$\kappa = B_n\left(\frac{L}{B_o}\right)^{1/2} W^{-1/4}$
Quasi Adiabatic Ions
Adiabatic
Wall
B_z
κ
B_n
2.0
1.0
0.5
0
-20
-40
-60
-80
-100
$X_{GSM}(R_E)$

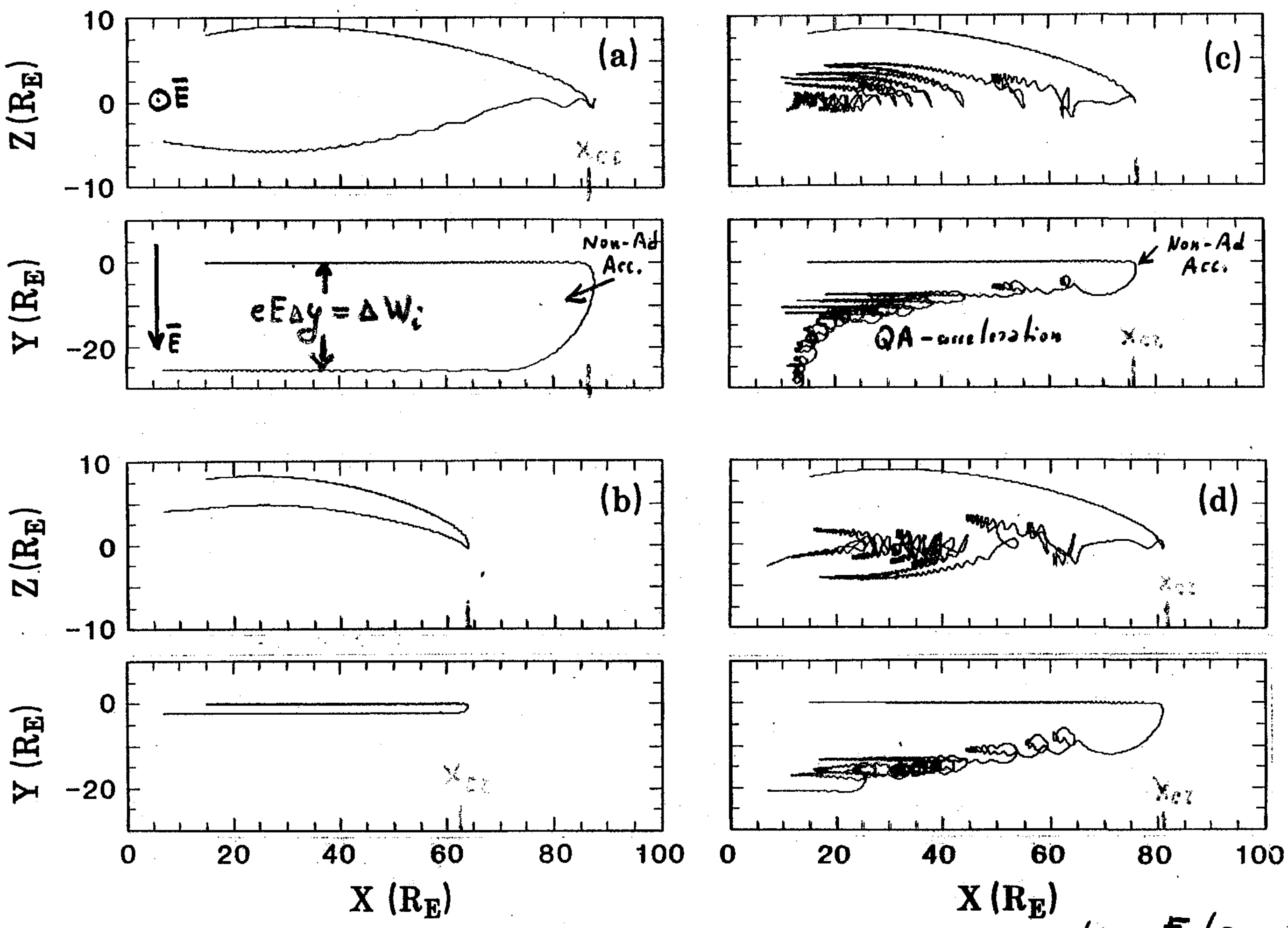

1. Non-Ad. Acceleration

2. QA acceleration — convection E/B
DRIFT → $\partial B/\partial x$

5

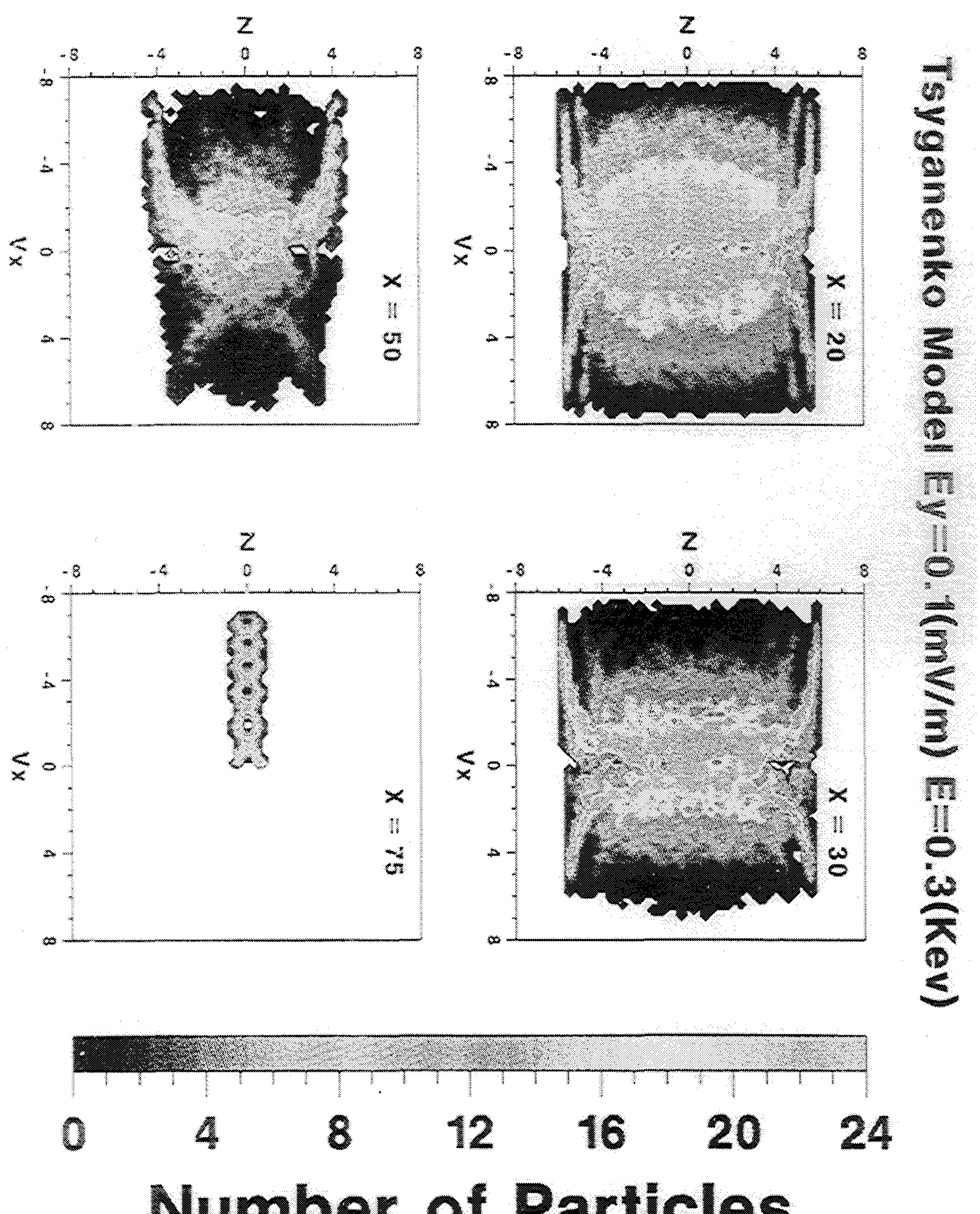

Tsyganenko Model Ey=0.1(mV/m) E=0.3(Kev)
X = 20
X = 30
X = 50
X = 75
Z
Vx
0 4 8 12 16 20 24
Number of Particles

Fluid approximation

Isotropic $\hat{p}_{ij}$

$$\vec{J}_{\perp} = \frac{\vec{B}}{|\vec{B}|^2} \times \vec{\nabla} p$$

Guiding center drift approximation

Anisotropic $\hat{p}_{ij}$

$$\vec{J}_{\perp} = \frac{\vec{B}}{|\vec{B}|^2} \times \left[\vec{\nabla} p + \frac{p_{II} - p_{\perp}}{B^2} \underbrace{\left(\vec{B}\ \nabla \vec{B}\right)}_{\sim 1/R_{curv}} \right]$$

Nonadiabatic approximation

Nongyrotropic $\hat{p}_{ij}$

$$\vec{J}_{\perp} = \frac{\vec{B}}{|\vec{B}|^2} \times \left[\vec{\nabla} \hat{p}_{ij} \right]$$

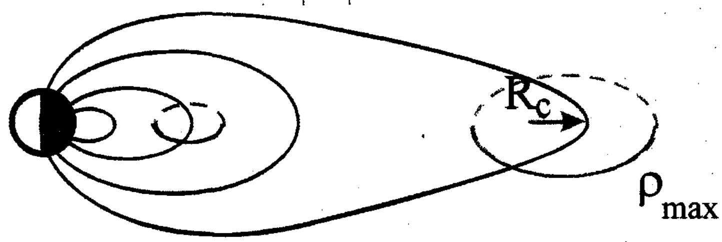

$$\kappa = \sqrt{R_c / \rho_{max}} << 1$$

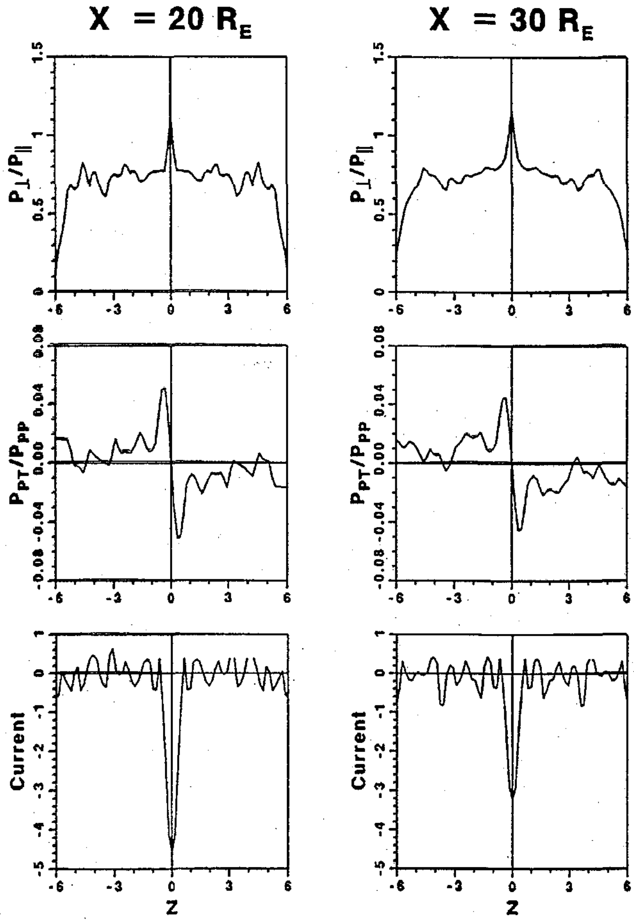

Figure 9. Profiles of the (top) pressure anisotropy, (middle) off-diagonal pressure P_{PT}/P_{PP} and (bottom) and transverse current j_y at $x = 20R_E$ (left-hand column) and $x = 30R_E$ (right-hand column). This figure shows that the region of $\delta \sim 1$ near $z = 0$ coincides with the region of significant off-diagonal terms and large transverse current.

we can write (32) for current in terms of $P_{xz}^{\max}$

$$j_y(z=0) = \frac{c}{B_n}\frac{P_{xz}^{\max}}{d_{xz}} \tag{33}$$

From (33) we can relate the value $P_{xz}^{\max}$ to the magnetic field at the edge of the current sheet

$$P_{xz}^{\max} = \frac{B_n B_x(z=d_{xz})}{4\pi}$$

Finally, we reduce this equation to a dimensionless form to compare it with the previous results. Using (29) we get

$$\frac{P_{xz}^{\max}}{P_{zz}} = 2\delta(x,z)\frac{B_n B_c(z=d_{xz})}{B_0^2 - B_x^2(z=d_{xz})} \tag{34}$$

In Figure 11b we plot two curves showing variation in the left and right sides of (34) with x. Once again, the solid line in this figure corresponds to $P_{xz}^{\max} / P_{zz}$ (left-hand side of (34)), and the dotted line corresponds to the right-hand side of (34). There is good agreement between the two curves, and we can conclude that the off-diagonal terms obtained in our model can maintain the necessary stress balance condition reasonably well.

The results of the estimates shown in this section are that the distribution we obtained is not too far from being in equilibrium. We do not expect the force balance condition to be exactly satisfied. The aim of these estimates was to show that the distribution of anisotropies, currents, and off-diagonal terms are fairly consistent with each other. These current distributions could also serve as a first iteration toward obtaining self-consistent equilibria. We believe that such an iterative approach (also used in other papers [e.g., *Burkhart et al.*, 1992] is more natural than

Structure of the PRESSURE tensor in MAGNETOTAIL

- $p_\perp > p_\parallel$ - adiabatic region
- $p_\perp \approx p_\parallel$ - pressure isotropy
- ✱✱✱✱ - off-diagonal terms!

Magnetic Field Model (Tsyganenko, 1989)

($k_p = 1^-, 1, 1^+$, Tilt = 0)

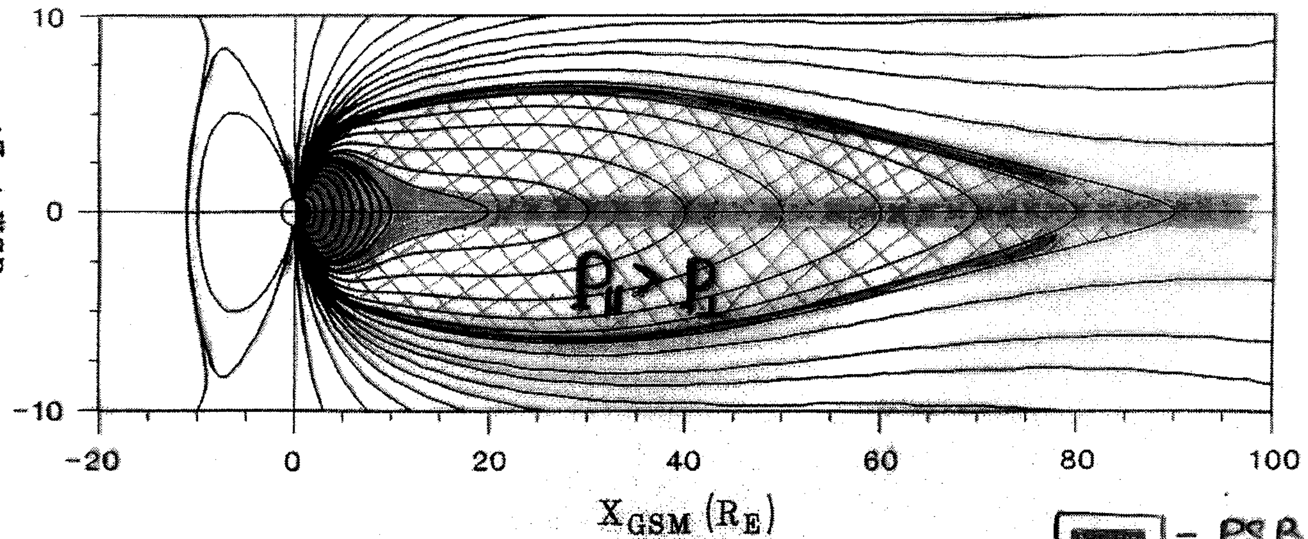

- PSBL ($p_\parallel \gg p_\perp$)

$p_\parallel \cong p_\perp + \frac{B^2}{4\pi} > p_\perp$ (MFC) QUASIADIABATIC region

Figure 2

A-G95-76

CLASSIFICATION OF MAGNETOTAIL ION VELOCITY DISTRIBUTIONS

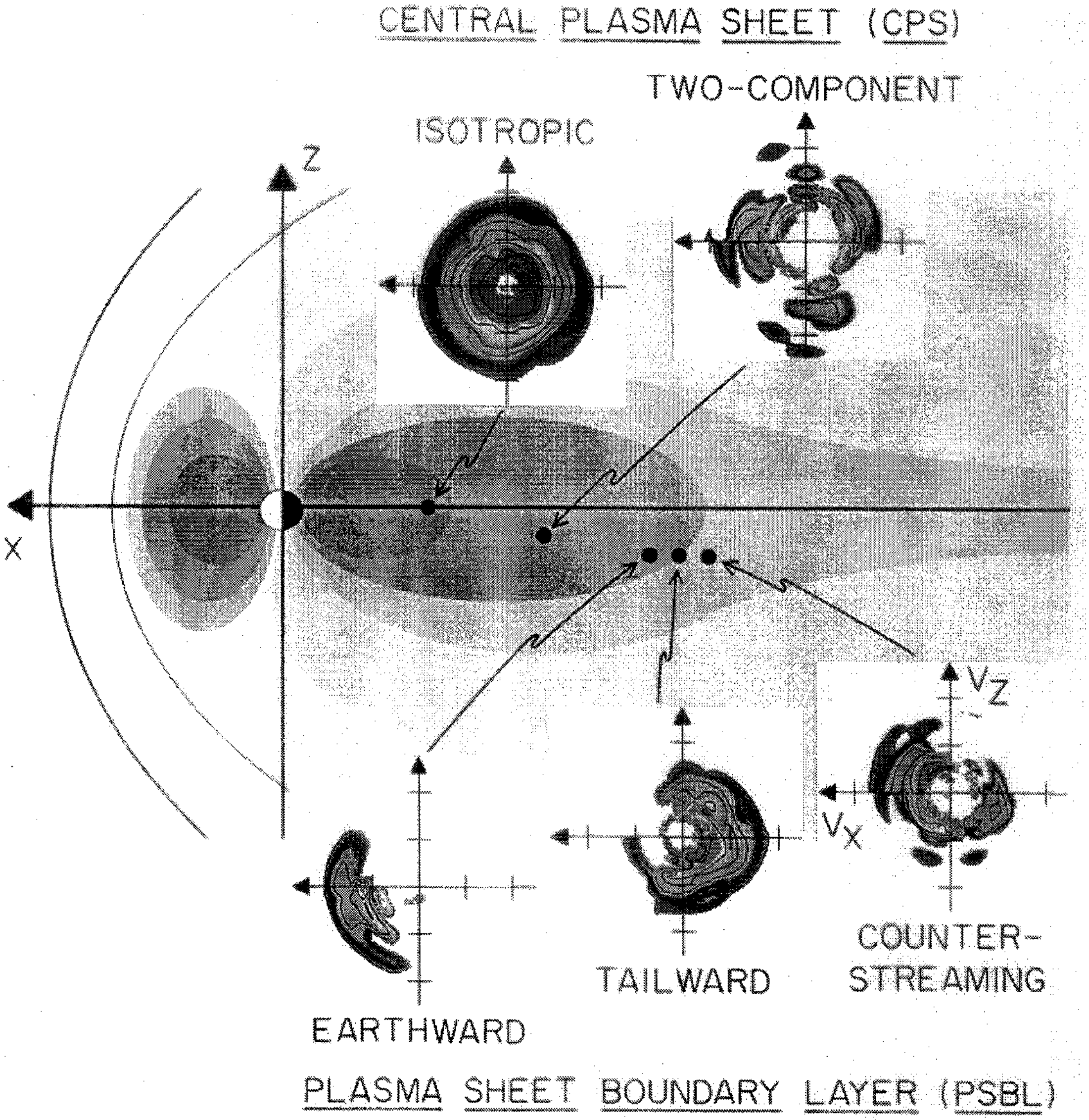

SEPARATRIX: $\kappa \ll 1$

FAST VARIABLES

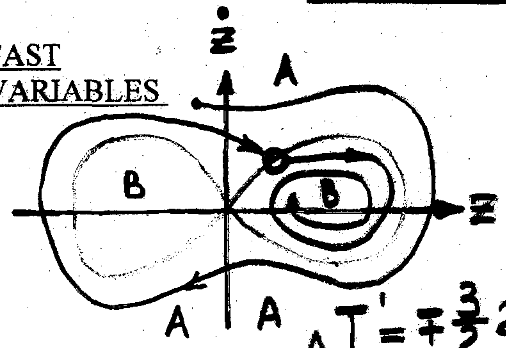

A - "Meandering" motion: particles cross **Z=0**

B – "Guiding" center motion: no crossings **Z=0 plane**

$$\Delta I' = \mp\frac{3}{2}\varkappa\left(1-(I')^{4/3}\right)\ln\left|2\sin\theta_s\right|$$

θ_s – phase of "fast" oscillations = $\int_0^{t=t_s}\omega_z\,dt$

Timofeev
Neistadt
Gary, Escander,
Tennyson

Linear dependence on parameter of smallness:

$$|\Delta I'| \sim \varkappa < 1 \quad \left(\Delta\mu \sim \exp(-\varkappa_c^2),\ \varkappa_c >> 1\right)$$

SLOW VARIABLES:

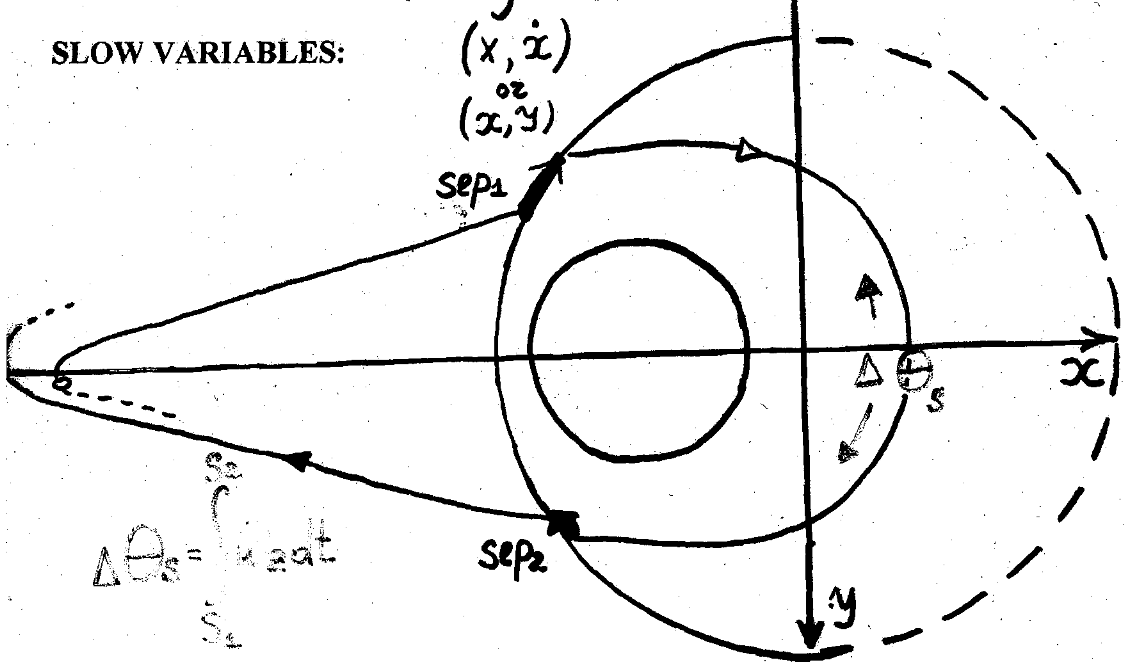

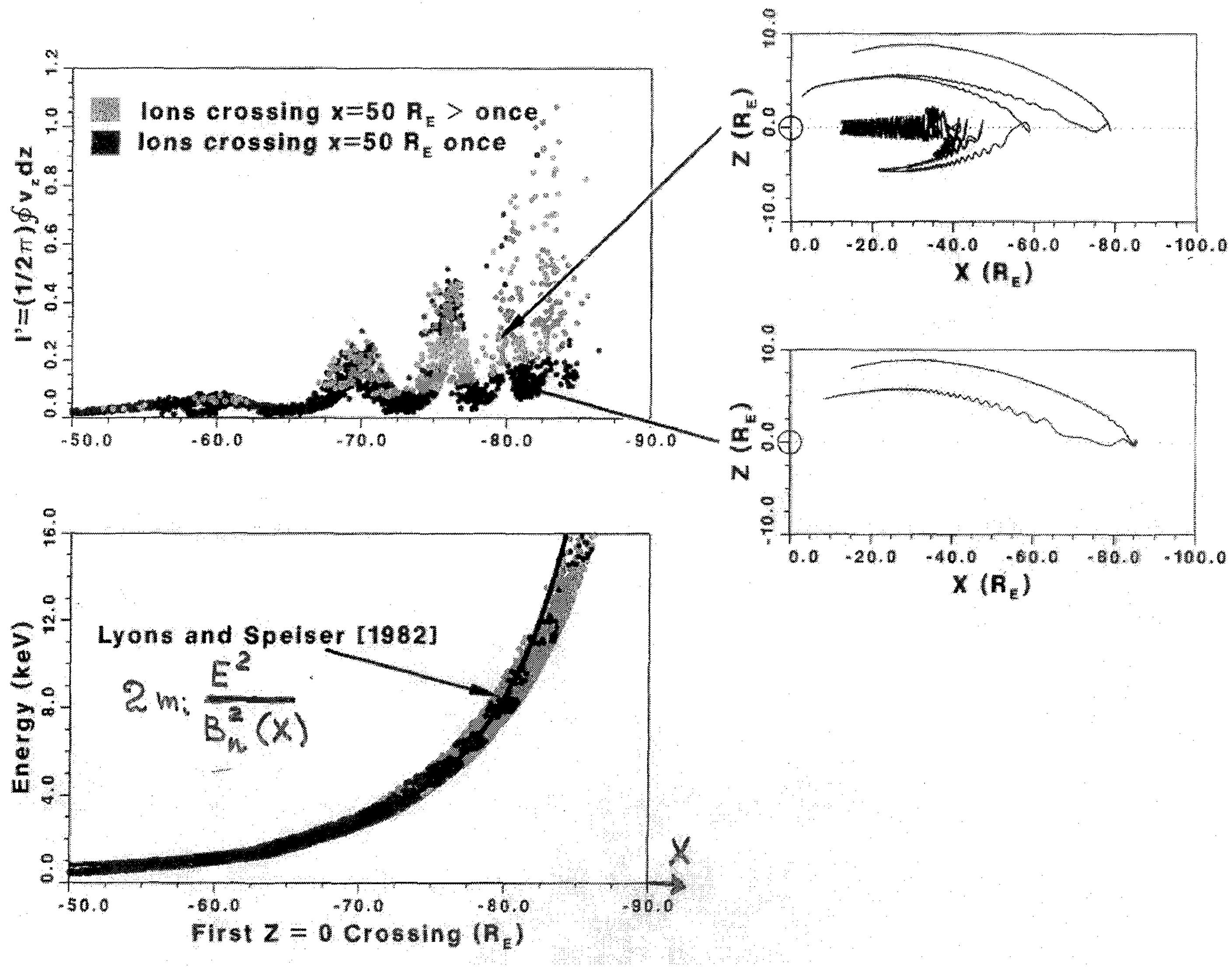
Ions crossing x=50 R_E > once
Ions crossing x=50 R_E once
I'=(1/2π)∮v_z dz
-50.0 -60.0 -70.0 -80.0 -90.0
Z (R_E)
X (R_E)
0.0 -20.0 -40.0 -60.0 -80.0 -100.0
Lyons and Speiser [1982]
2 m_i E²/B_n²(X)
Energy (keV)
First Z = 0 Crossing (R_E)
X

Time-dependent Self-Consistent Large-Scale Kinetic Model

- What is the effect of non-adiabatic ions on the overall structure of the magnetotail?

- How does the magnetotail adjust to changes in external parameters (e.g. changes in the solar wind).

- Role of electron currents and $\nabla\varphi(\bar{r},t)$ on magnetotail structure and dynamics.

Caution: *This is not a particle code, but allows us to examine ion dynamics on a global scale.*

Kinetic models $\longleftrightarrow$ MHD models

• There are Naturall <u>SPATIAL</u> and <u>TEMPORAL</u> THRESHOLDS on application of MHD results

$$\lambda > \lambda^* \qquad \tau > \tau^*$$

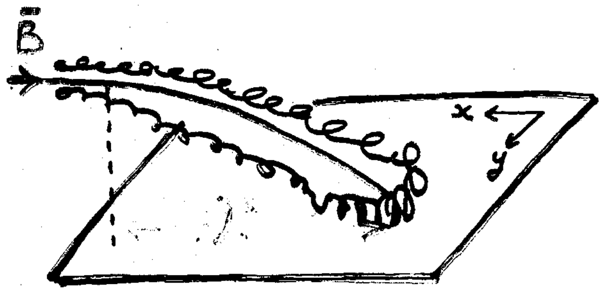

$\lambda^* \sim \rho_i \rightarrow \rho_i^{eff}$

ρ_i^{eff} - scale of non-Adiabatic orbit

• Self-Consistent LSK 1997 …

- • smalll scale structuring ?
- • transient features ?

◉ <u>How kinetic effects could control Large Scale Structure ?</u>

METHODOLOGY

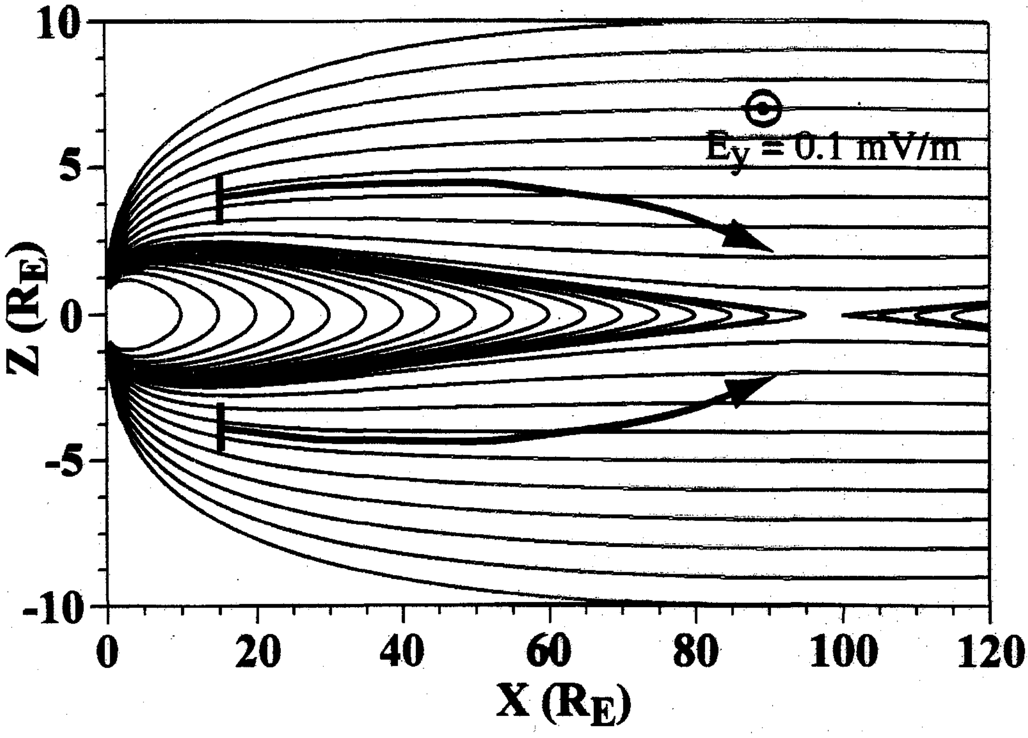

- **Launch ions continuously from a plasma mantle source from both hemispheres in modified *Birn-Zwingmann* magnetic field model.**
- **Populate magnetosphere for 1 hour.**
- **Update B using Biot-Savart Law.**
- **Continue launching and update B every 30 seconds.**
- **Calculate inductive electric field (~ order of cross-tail field) for each interval and add to model.**

SIMULATION TIMELINE

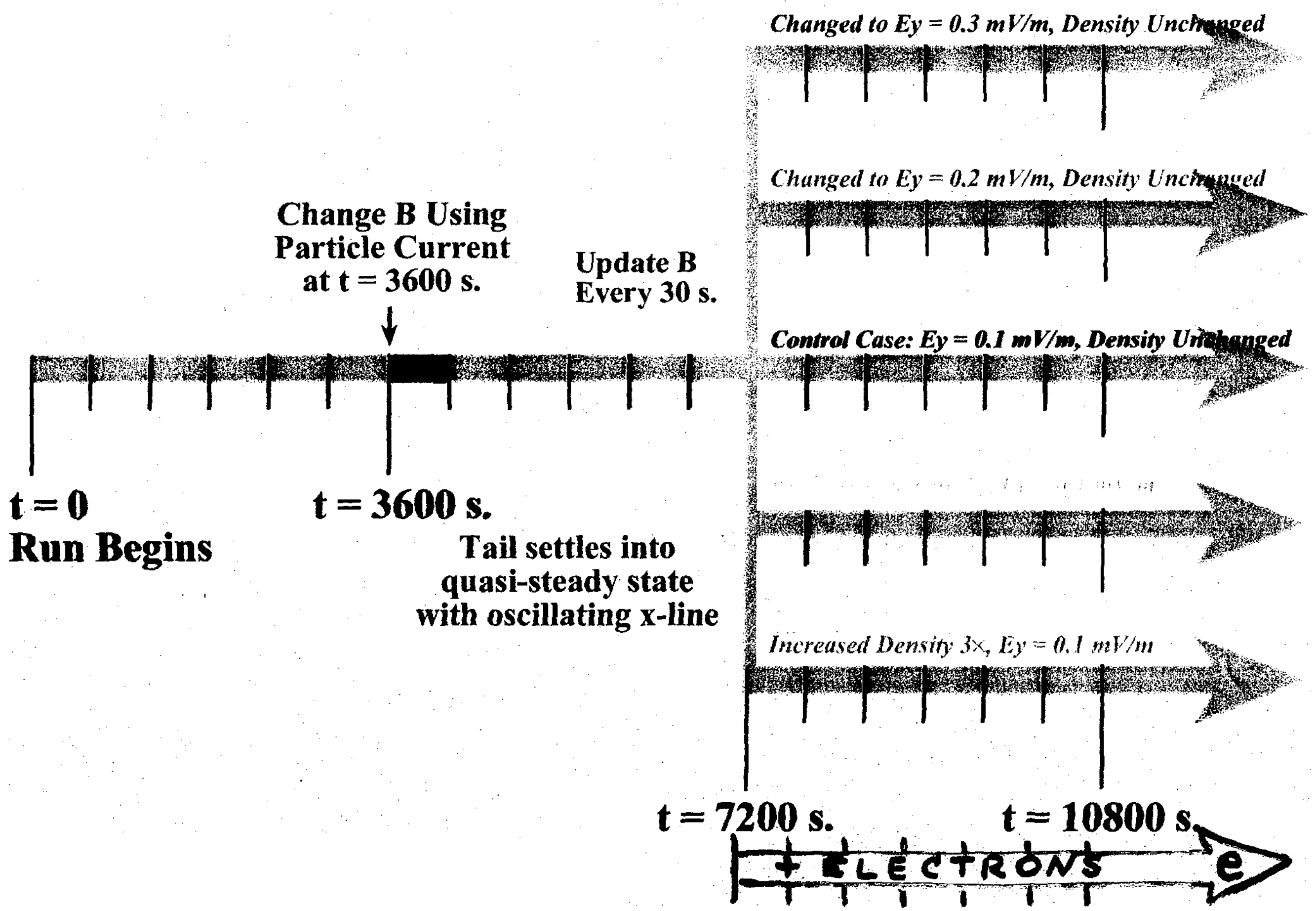

Time Evolution of Magnetic Field

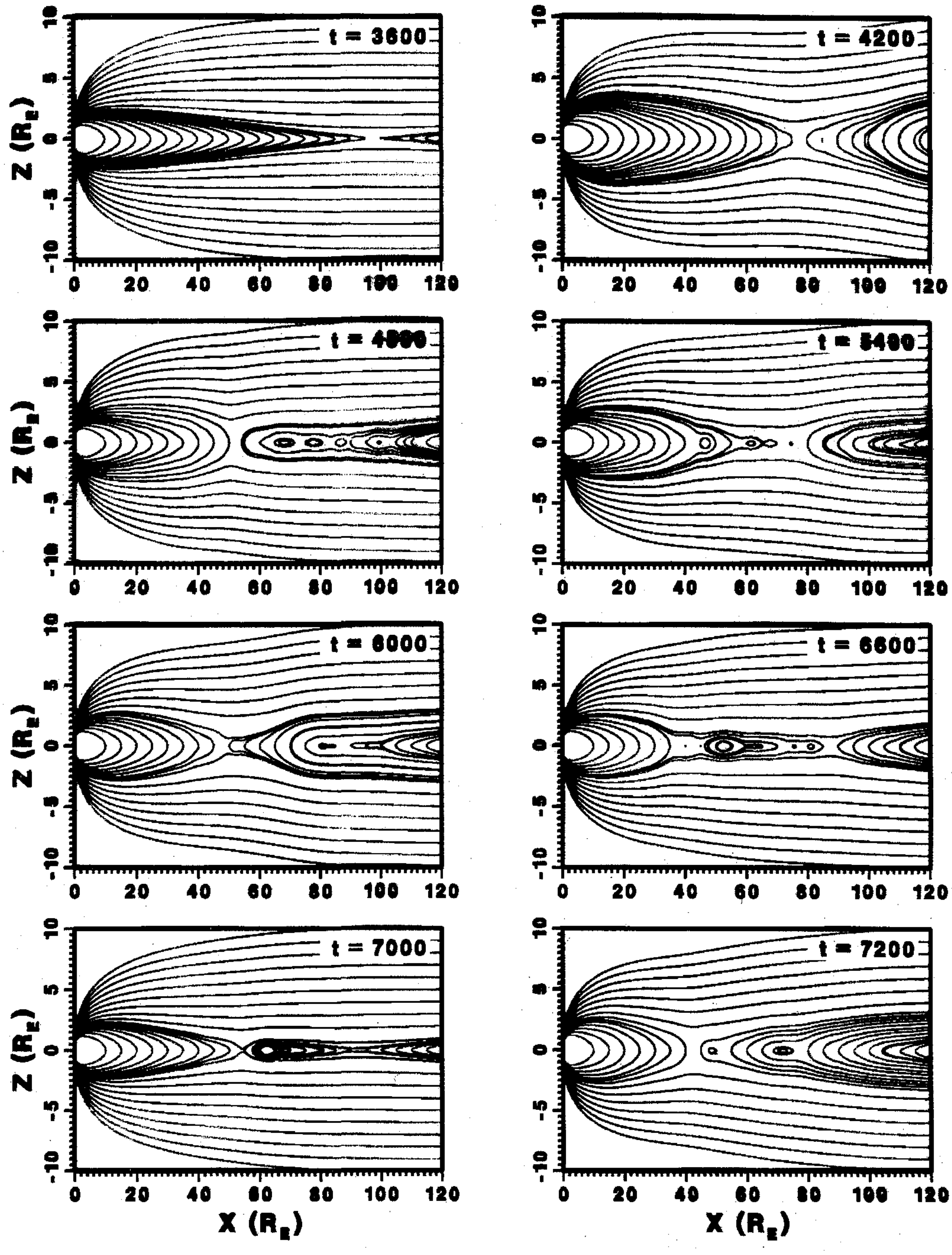

Time Evolution of Particle Current

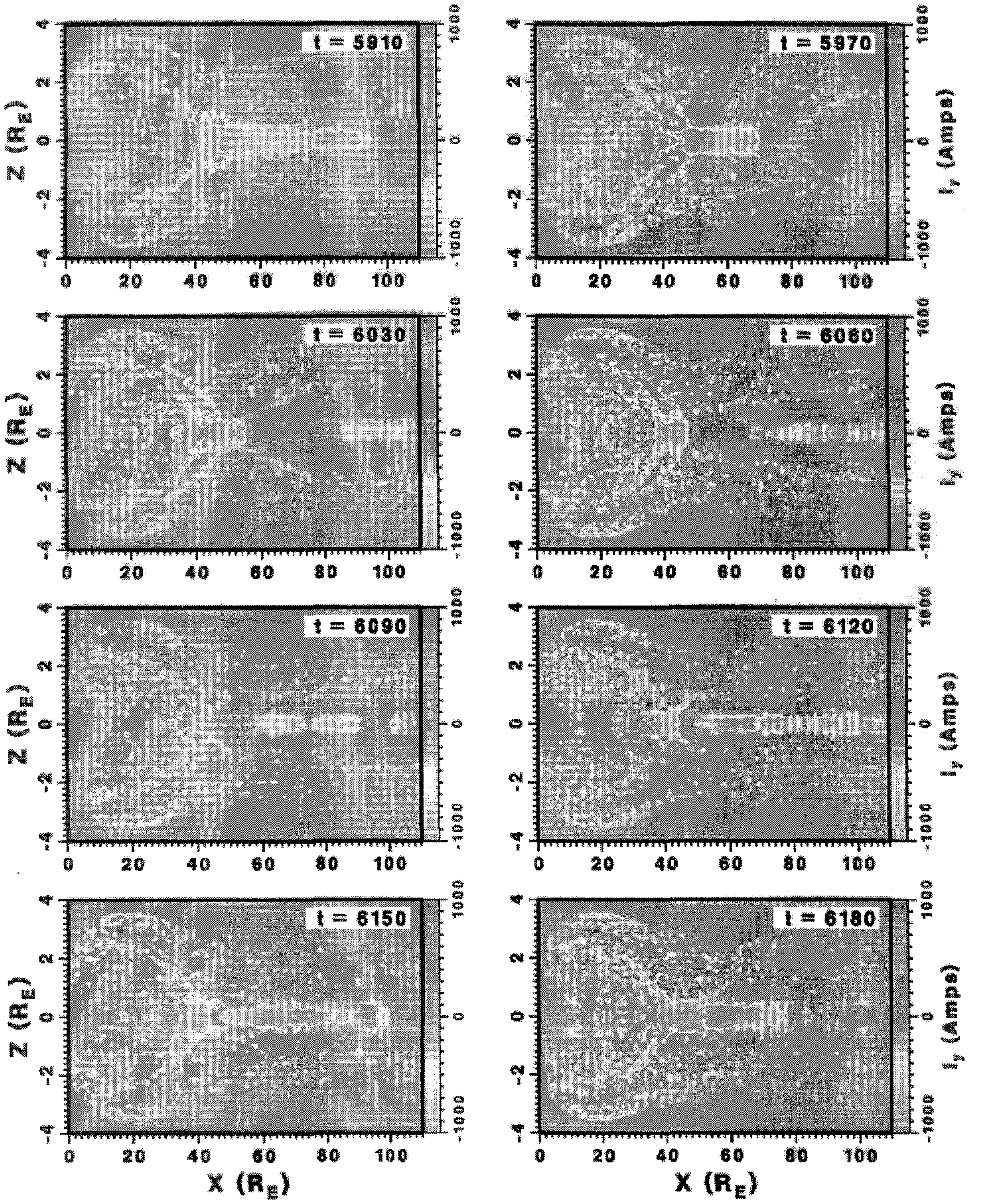

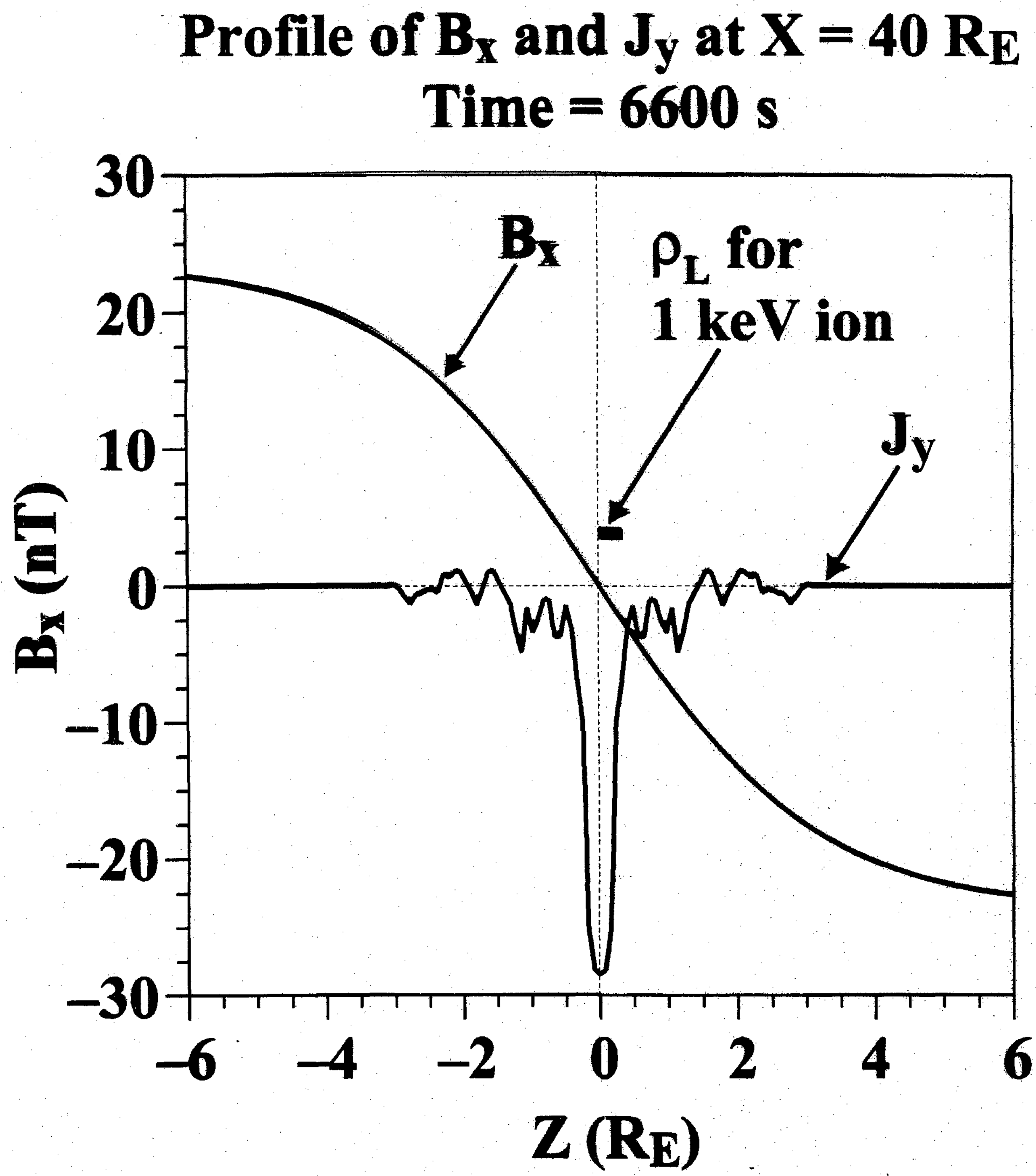

Profile of B_x and J_y at X = 40 R_E
Time = 6600 s
B_x
ρ_L for
1 keV ion
J_y
B_x (nT)
30
20
10
0
–10
–20
–30
–6
–4
–2
0
2
4
6
Z (R_E)

Variability in the Magnetotail

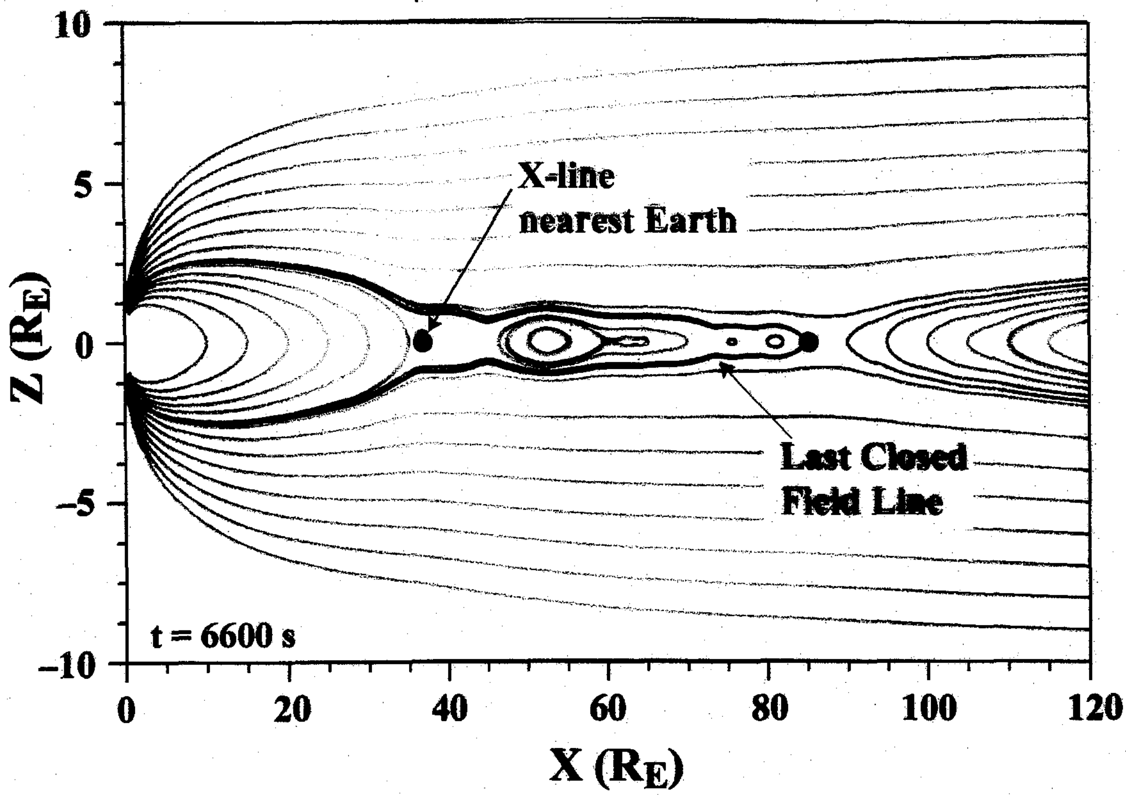

- **Will use location of equatorial crossing of last closed field line (black dot) and location of X-line nearest Earth (red dot) as gauge of variability in the tail.**

MOTION OF THE X-LINE IN THE MAGNETOTAIL

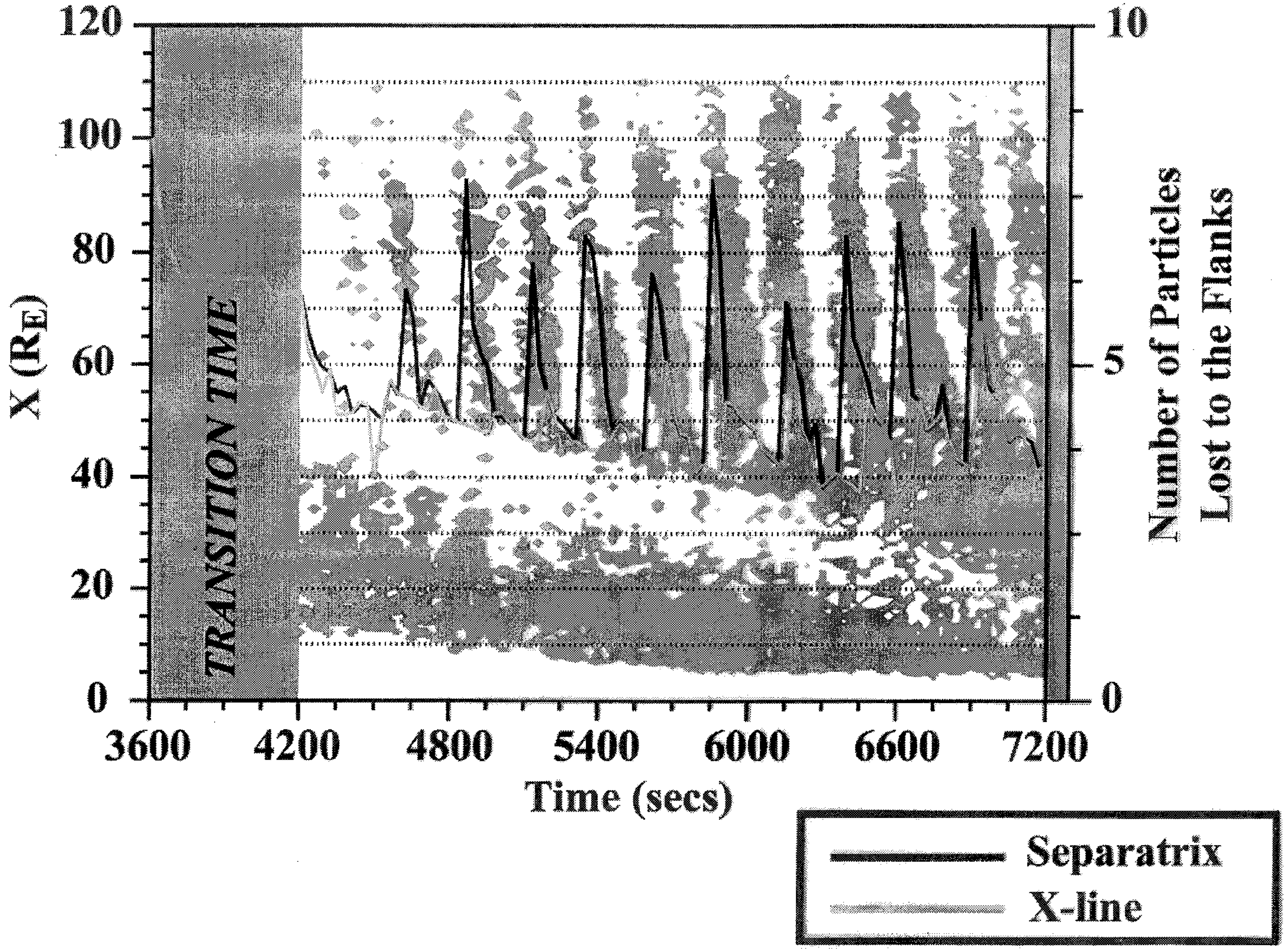

TRANSIENT DISRUPTIONS

of magnetotail cross-tail current (selfconsistent regime)

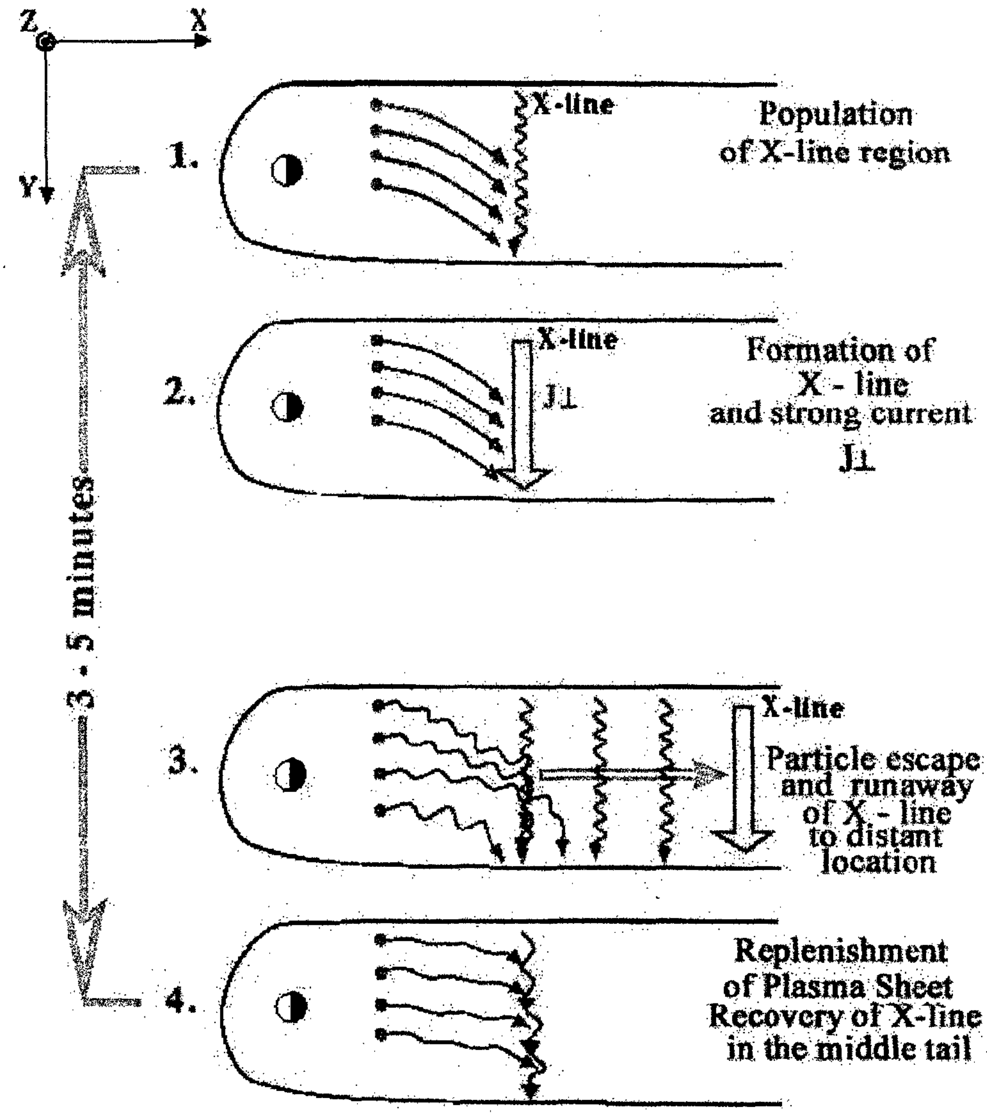

Summary of Variability

Carried out a 2-D self-consistent, time-dependent LSK simulation of the magnetotail.

- Tail evolves into quasi-steady state in which the location of X-line oscillates between $x \sim 40\ R_E$ and $x \sim 60\ R_E$.

- Oscillations are caused by depletion of plasma in the central portion of the distant tail because of non-adiabatic ion dynamics and the associated changes in the current sheet.

- Intrinsic variability may explain "flow turbulence" seen in spacecraft observations.

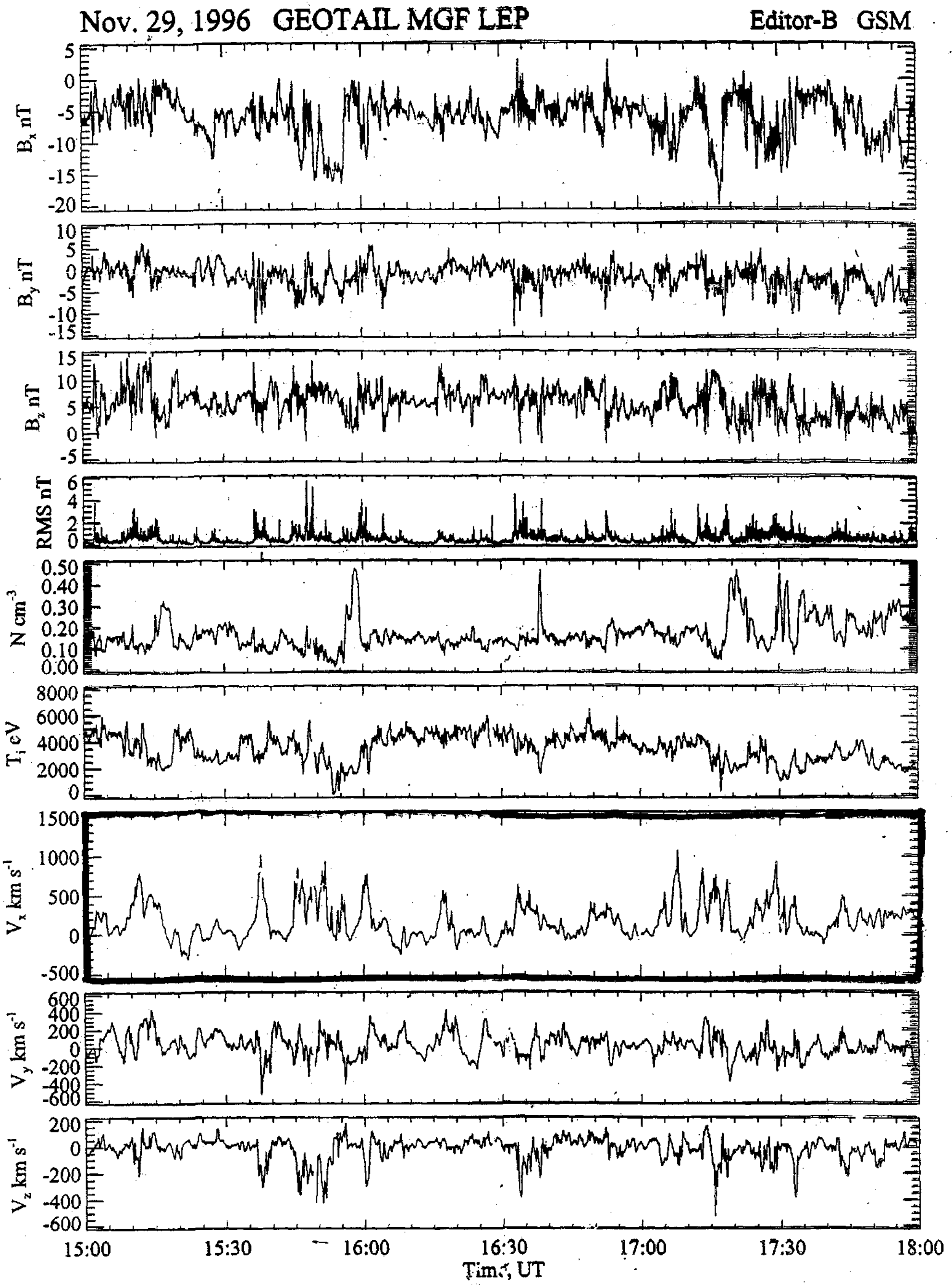

Created by the DARTS system at ISAS, Japan

Magnetotail is populated by
SW (ionospheric) plasma $\qquad N_0$ $^{part}/_s$

Magnetotail convection is driven
by SW flow around magnetosphere $\qquad \underline{E_y}$ $^{mV}/_m$
$E = -\,^1/_c\,[\,\bar{V} \times \bar{B}\,]$

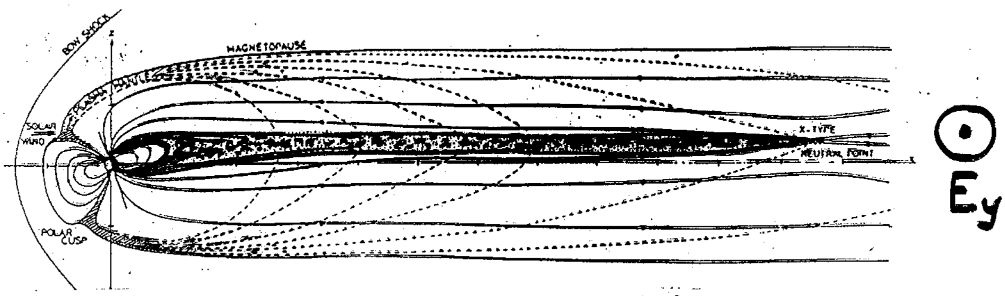

N_0 and $\underline{E_y}$ are independent parameters **!**

Is steady State Solution Always Possible?

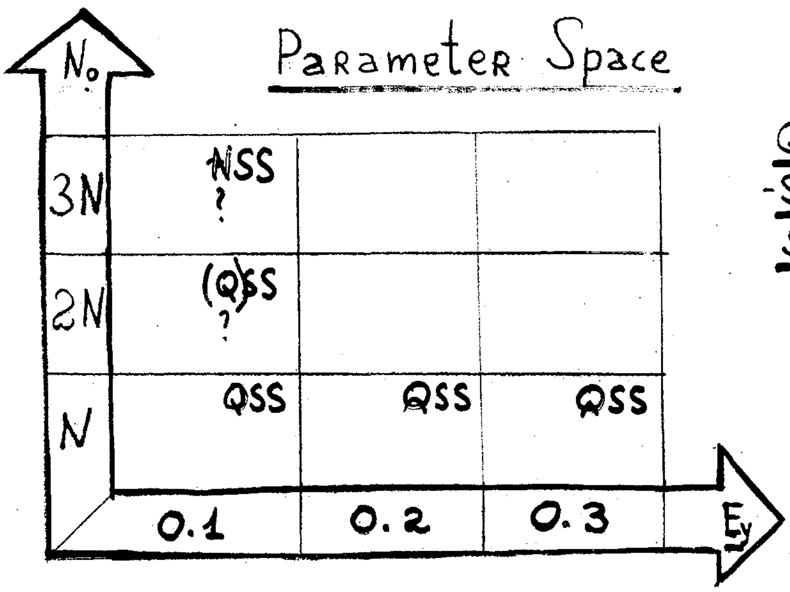

Quasi-
-**S**teady
State

Increase of the Plasma Mantle Influx

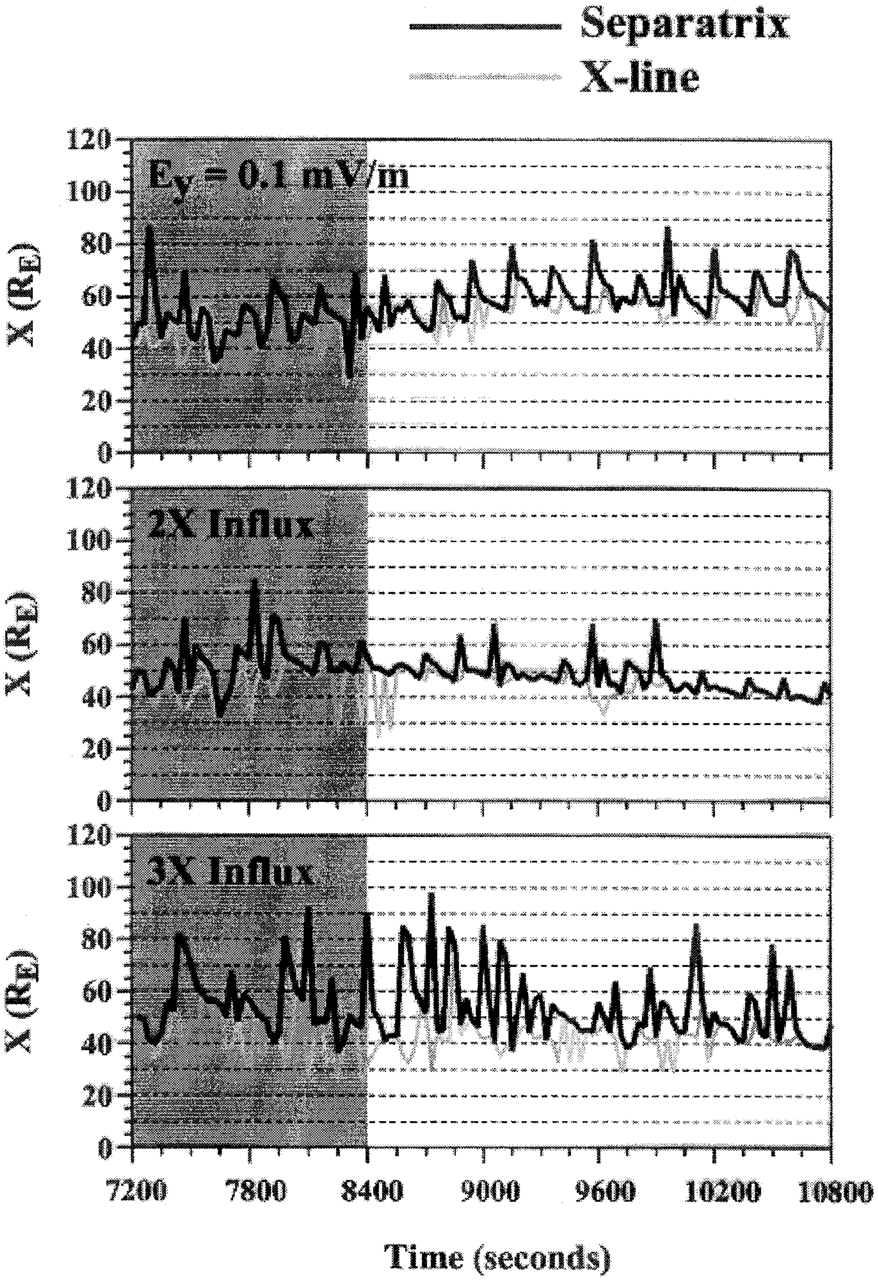

Closest to Equilibrium state

System Overpopulated

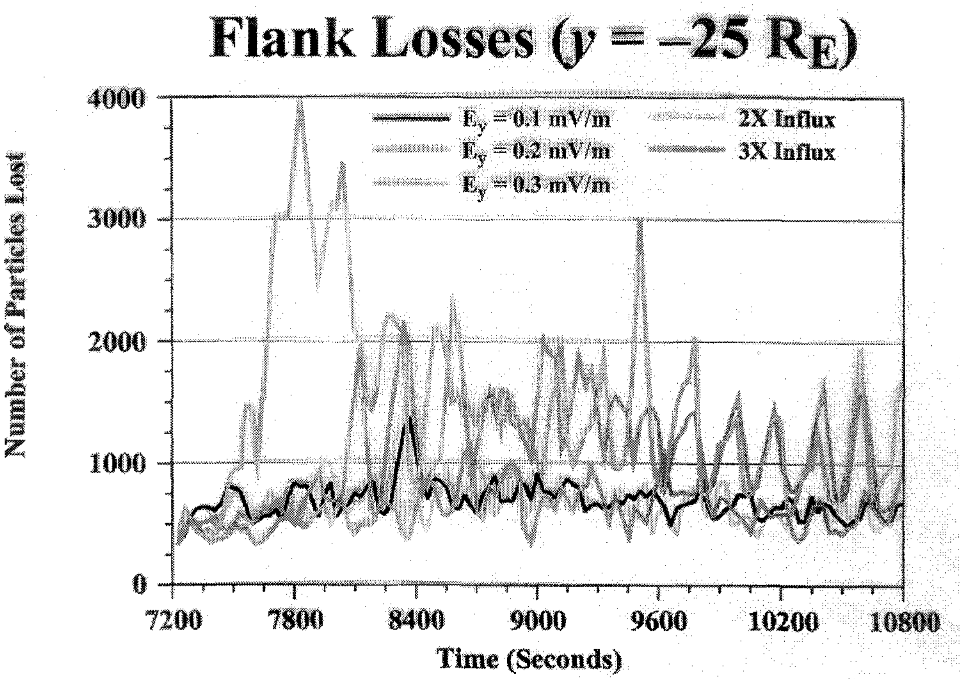
Flank Losses ($y = -25\ R_E$)
E_y = 0.1 mV/m
E_y = 0.2 mV/m
E_y = 0.3 mV/m
2X Influx
3X Influx
Number of Particles Lost
0
1000
2000
3000
4000
7200
7800
8400
9000
9600
10200
10800
Time (Seconds)

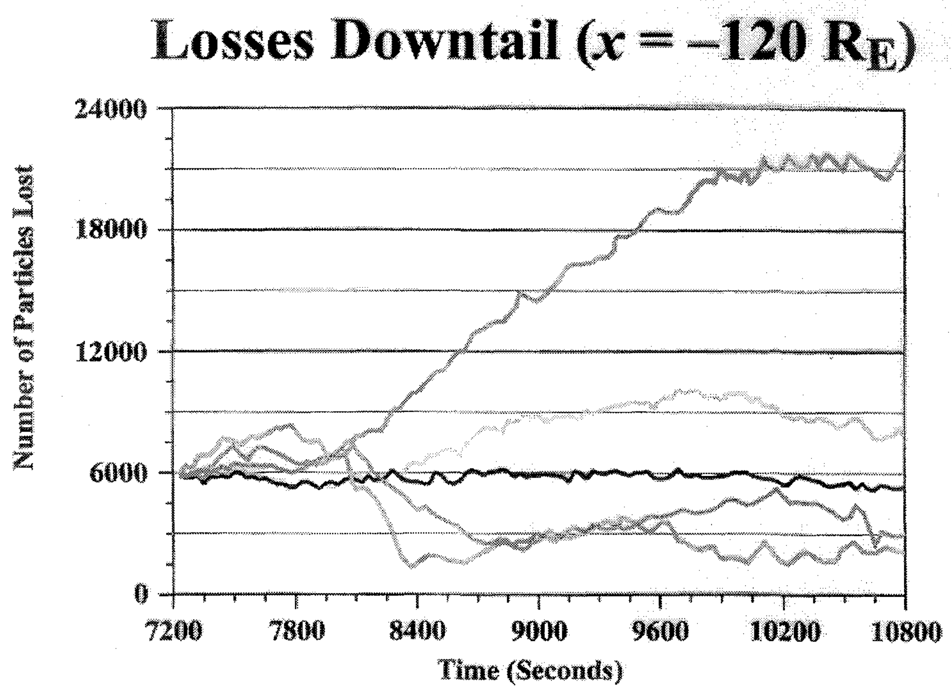
Losses Downtail ($x = -120\ R_E$)
Number of Particles Lost
0
6000
12000
18000
24000
7200
7800
8400
9000
9600
10200
10800
Time (Seconds)

Response of the Magnetotail to Overpopulation

Original Run

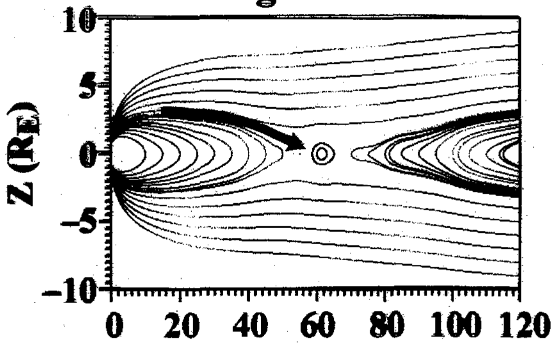

Sources and losses balanced by X-line motion

2X Influx

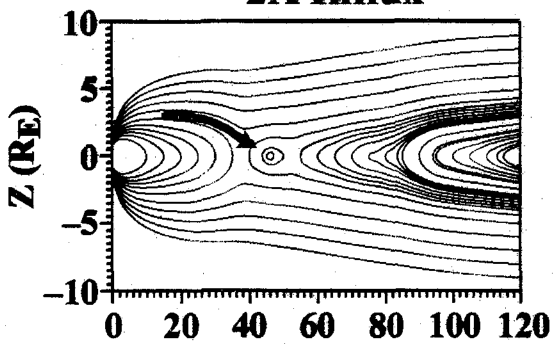

Magnetotail balances itself by trapping particles Earthward of weak field region (X-line motion damped).

3X Influx

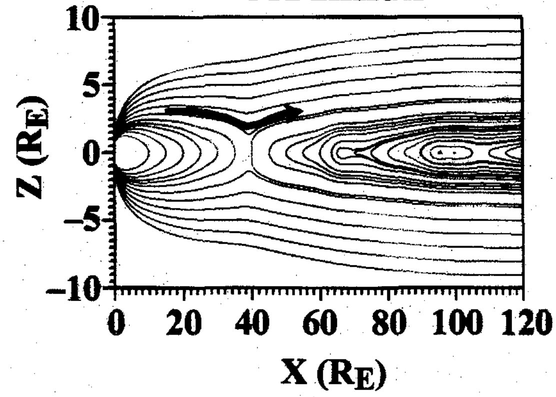

Overpopulation results in large currents in distant tail: Plasma mantle has less access to current sheet

Summary of Self-Adjustment

Carried out a parameter search by varying the cross-tail electric field and the plasma mantle particle influx rate.

- Increase of the cross-tail field results in faster loss of particles. Process saturates since the replenishment rate is unaffected. X-line moves closer to Earth.

- Increase of particle influx causes flaring of the tail, resulting in the loss of ion access to the distant tail current sheet.

Increase of the Cross-Tail Electric Field

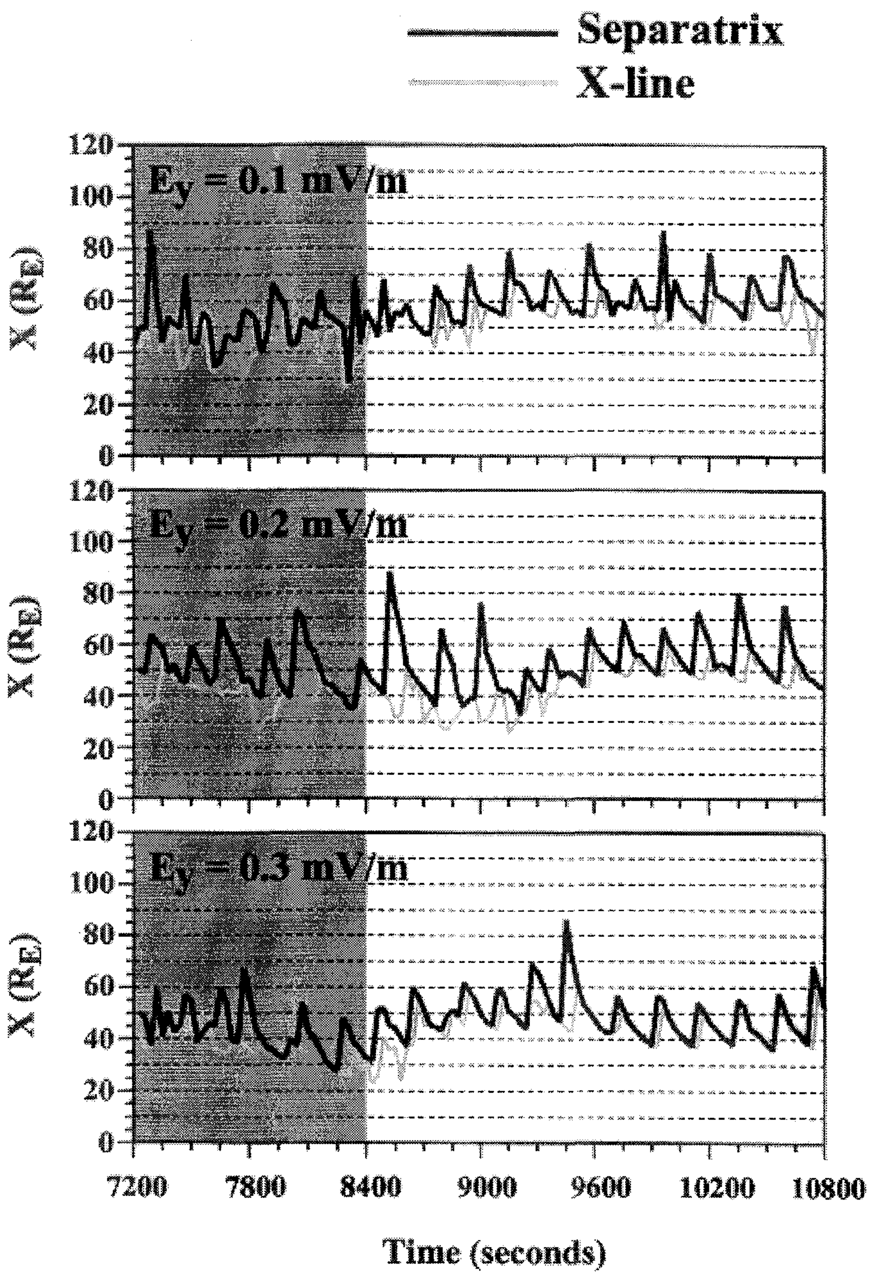

Average Period of Oscillation: 270 s.

Average X-line Position: 51.3 R_E

Average Period of Oscillation: 216 s.

Average X-line Position: 43.3 R_E

Average Period of Oscillation: 210 s.

Average X-line Position: 42.4 R_E

Self-consistent LSK modeling of magnetotail.

INCLUSION OF ELECTRON CURRENTS

We assume that we can use the **fluid** approximation for the *motion* of electrons and write

transverse motion
$$m_e \frac{d\vec{V}_{e\perp}}{dt} = -e\left(\vec{E} + \frac{\vec{V}_e \times \vec{B}}{c}\right)_{\perp} - \frac{\nabla_{\perp} P_e}{n_e} \quad (1a)$$

parallel motion
$$m_e \frac{dV_{e\parallel}}{dt} = -eE_{\parallel} - \frac{\nabla_{\parallel} P_e}{n_e} - \mu \nabla_{\parallel} B \quad (1b)$$

Neglecting electron inertia (slow processes: $\tau \geq 1$-2min) and assuming $\vec{E} = -\nabla \varphi$:

$$\vec{V}_{e\perp} = c\frac{\vec{E} \times \vec{B}}{B^2} + c\frac{\nabla_{\perp} P_e \times \vec{B}}{en_e B^2} \quad (2a)$$

$$e\nabla \varphi - \frac{\nabla_{\parallel} P_e}{n_e} - \mu \nabla B = 0 \quad (2b)$$

Assuming **isothermal** Equation of State for the electron component

$$P_e \approx n_e T_e = c_0 n_e^{\gamma} \qquad \gamma = 1 \quad (3)$$

and **quasineutrality** condition

- $n_i(s, x_0) = n_e(s, x_0)$ (4)

Eqs **(2b) - 4** give the **Boltzmann** relation along field lines:

- $$n_i(s,x_0) = n_e(s,x_0) = n_e(0,x_0)e^{\left[-\frac{U(s,x_0)}{W_e(x_0)}\right]} \qquad \text{(5a)}$$

$$U(s,x_0) = \mu B(s,x_0) - e\varphi(s,x_0) \qquad \text{(5b)}$$

We could solve Eq.**(5)** for the potential $\varphi(s,x_0)$:

$$\varphi(s,x_0) = \frac{1}{e}\left\{\underbrace{\mu B(s,x_0)}_{\textit{MIRROR TERM}} + \underbrace{W_e(x_0)\ln\left[\frac{n_i(s,x_0)}{n_i(0,x_0)}\right]}_{\textit{PRESSURE TERM}}\right\} \qquad \text{(6)}$$

$n_i(s,x_0)$ is determined from the kinetic calculations of ion trajectories

$W_e(x_0) = const$ - electron energy

We obtain $\underline{E_\perp^{(pot)} = -\nabla_\perp\varphi \, , \; E_\parallel = -\nabla_\parallel\varphi}$ (7)

due to electron motion everywhere in the system.

Free Parameters

$W_e(x_0)$	Take as $T_e = 250$ eV, constant throughout system.
$V_{e\perp}/V_{e\parallel}$	(Used for μ) Vary between 0.0 to 0.2

Electron currents:

$$J_{\perp e} = -en_i V_{e\perp} \tag{8}$$

- $$\vec{V}_{e\perp} = -c\frac{\left[(\nabla_\perp \varphi)\times \vec{B}\right]}{B^2} + c\frac{W_{e0}\left[\nabla_\perp (\ln n_i(s,x_0))\times \vec{B}\right]}{eB^2} \tag{9}$$

Distribution of n_i - ion trajectory calculations

Distribution of φ - Eq. **(6)**

Total electric field:

- $$\underline{\vec{E}_\Sigma} = \underbrace{E_0\vec{e}_y}_{\text{Dawn-dusk field}} + \underbrace{\vec{E}_{ind}}_{\sim \frac{\partial B}{\partial t}} + \underbrace{E_\parallel \vec{b} + \vec{E}_\perp^{(pot)}}_{\text{due to electrons}}$$

Transverse ion current $J_{\perp i}$ - ion trajectory calculations in the fields $\vec{E}_\Sigma(t), \vec{B}(t)$

Total current:

- $$\vec{J}_\perp = \vec{J}_{\perp e} + \vec{J}_{\perp i}$$

- Updating magnetic field:

$$rot\vec{B}(t) = -\frac{4\pi}{c}\vec{J}_\perp(t)$$

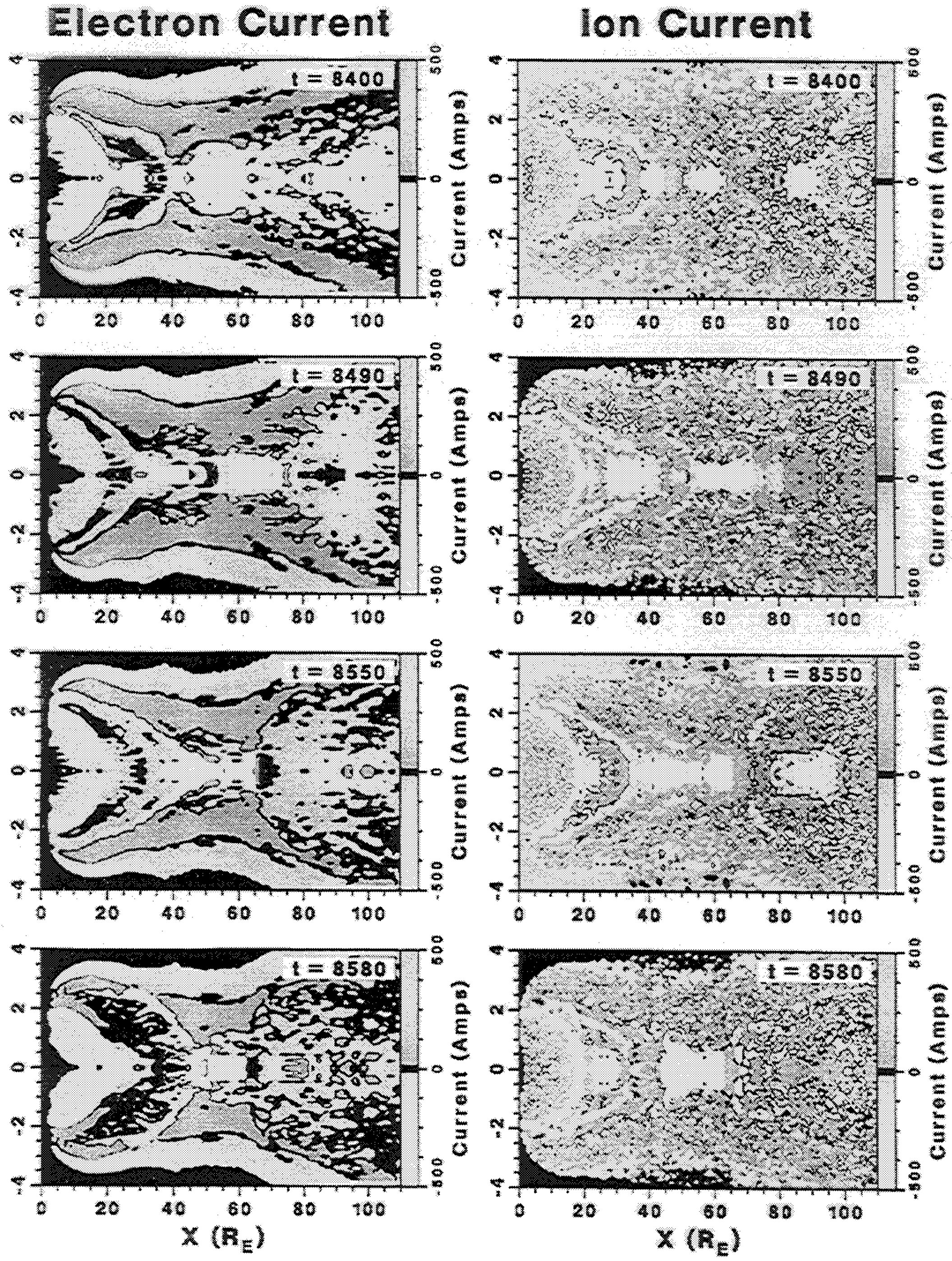

Electron Current
Ion Current
t = 8400
t = 8490
t = 8550
t = 8580
Current (Amps)
X (R_E)

Location of X-line vs. Time

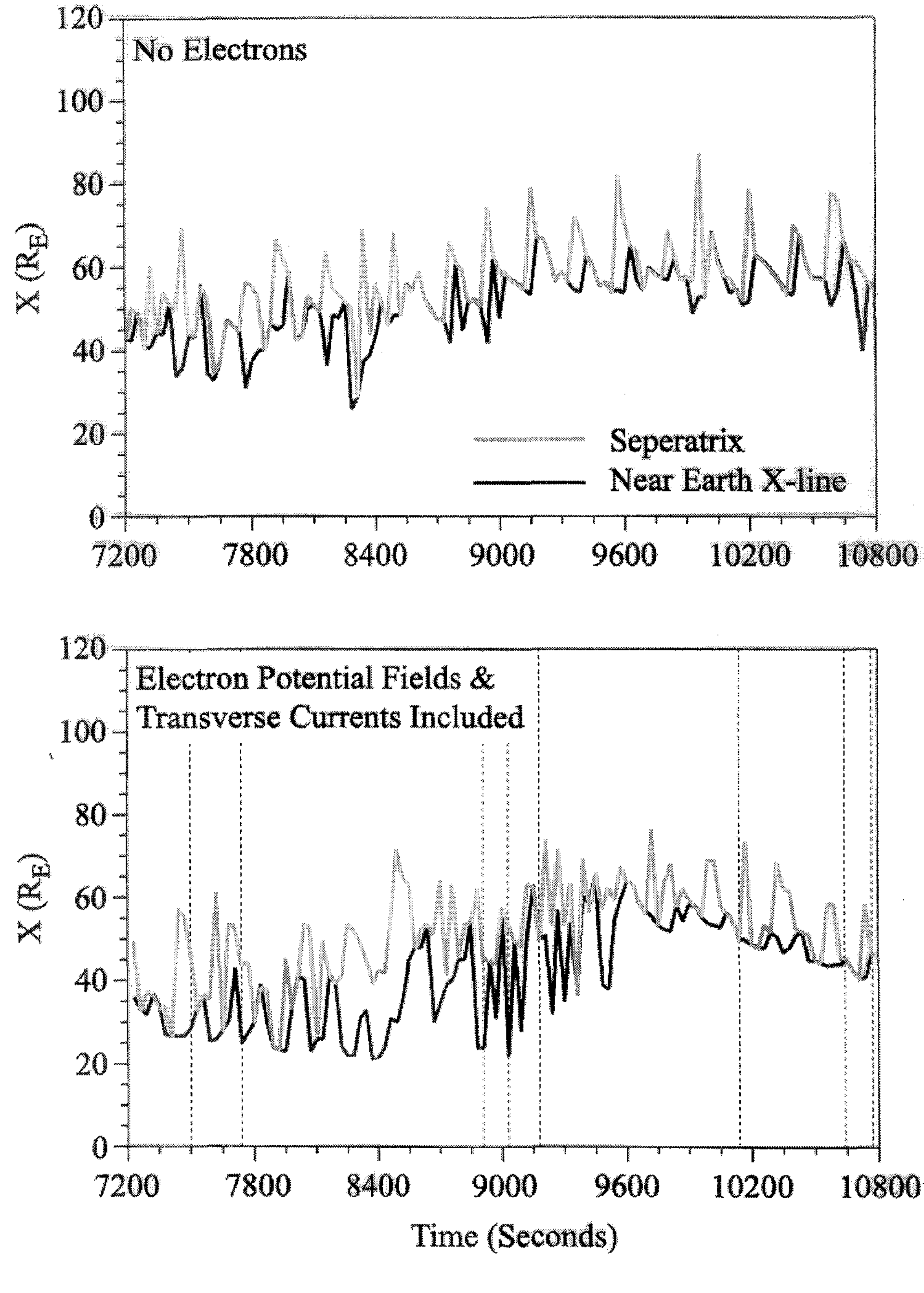

Standard Magnetotail Paradigm

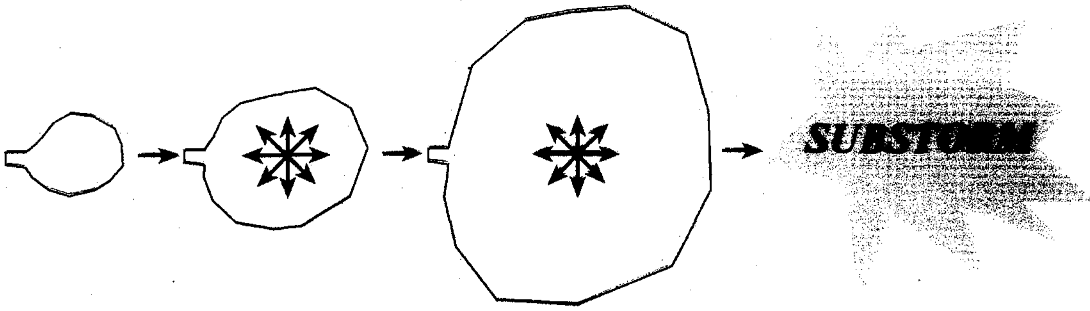

Magnetotail Self-Adjustment

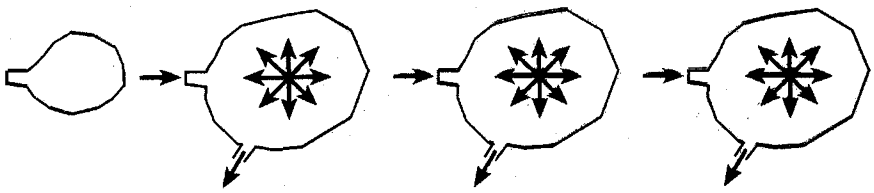

Magnetotail Overpopulation

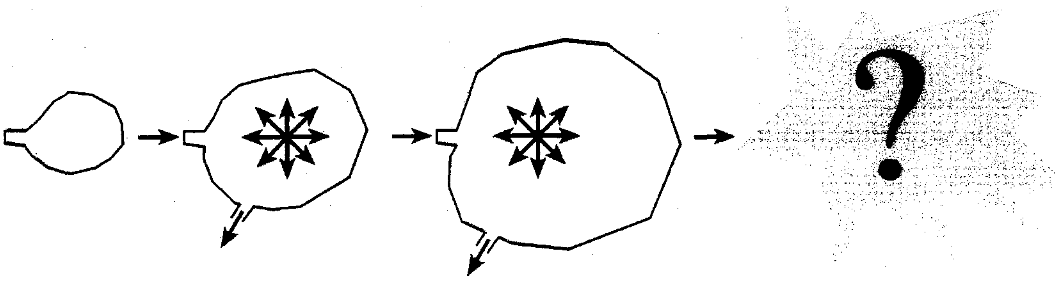

Summary:

- Magnetotail equilibrium is DYNAMIC

→ Balance of losses and Sources
occurs only on AVERAGE

Tail always (?) adjusts to the
OVERPOPULATION/UNDERPOPULATION
at large (tens of min) TIME SCALES

For smaller (minutes) scales it reaches **NESS**:
NON EQUILIBRIUM STEADY STATE
variable at $\tau \sim$ few min, $\lambda \sim$ fractions of R_E
(Reminds Syrovatsky's DYNAMIC Current Sheet model.)

Intrinsic Variability of Magnetotail is caused by
NonAdiabatic ion dynamics in the current sheet.
Electron effects do not modify NESS significantly
(at ion spatial/temporal scales)

REFERENCES for LECTURE 1

A. Results of Lecture 1 are published in following papers:

1. Büchner J., L.M.Zelenyi. Regular and chaotic charged particle motion in magnetotaillike field reversals 1. J. Geophys. Res., **94**, A9, 11812-11842, 1989.

2. Zelenyi L.M., A.A.Galeev, C.F.Kennel. Ion precipitation from the inner plasma sheet due to stochastic diffusion. J.Geophys.Res., **95**, A4, 3871-3882, 1990.

3 Ashour-Abdalla M., J.Berchem, J.Buechner, L.M.Zelenyi. Shaping of the magnetotail from the Mantle: Global and Local Structuring. J. Geophys. Res., (English edition), **98**, A4, 5651-5676, 1993.

4. Zelenyi L.M., B.V.Savenkov. Breakdown of quasiadiabaticity during the motion of particles in configurations with large curvature of magnetic field lines. Sov. J. Plasma Phys., (English edition), 19, 11, 1994.

5. Ashour-Abdalla M., L.M.Zelenyi, V.Peroomian, R.Richard, J.Bosqued. The mosaic structure of plasma bulk flows in the Earth's magnetotail. J. Geophys. Res., **100**, A10, 19191-19209, 1995.

6. Ashour-Abdalla M., L.Zelenyi, V.Peroomian, L.Frank, and W.Paterson. Coarse-grained texture of ion distributions in the magnetotail: A fractal-like approach. J.Geophys.Res., **101**, A7, 15287-15296, 1996.

7. Savenkov B.V., L.M.Zelenyi. Application of separatrix crossing theory to nondiffusion model of current sheet resonance. Geophys.Res.Lett., **23**, 22, 3255-3258, 1996.

8. Peroomian V., M.Ashour-Abdalla, L.M.Zelenyi. Intrinsic variability in the quiet-time magnetotail. AGU, Geophys.Monograph 118, Magnetospheric Current Systems, 305-312, 2000.

9. Peroomian V., M.Ashour-Abdalla, L.Zelenyi. Dynamical properties of self-consistent magnetotail configurations. J.Geophys.Res., **105**, A8, 18.807-18.818, 2000.

10. Peroomian V., L.M.Zelenyi. Large-scale kinetic modeling of magnetotail dynamics. Space Sci.Rev., 95, 257-271, 2001.

11. Sergeev V.A., J.-A.Sauvaud, D.Popescu, R.A.Kovrazhkin, V.N.Lutsenko, L.M.Zelenyi, et al.. Plasma sheet ion injections into the auroral bulge: Correlative study of spacecraft and ground observations. J. Gheophys. Res., **105**, A8, 18.465-18.481, 2000.

B. Additional important publications:

1. Ness N. F. The Earth's magnetic tail. J. Geophys. Res., 70, 2989, 1965.

2. Pilipp, W. G., G. Morfill. The formation of the plasma sheet resulting from plasma mantle dynamics. J. Geophys. Res., 83, 5670, 1978.

3. Speiser T. W. Conductivity without collisions or noise. Planet.Space Sci.,18, 613, 1970.

4. Speiser T. W. Particle trajectories in model current sheets; 1. Analytical solutions. J. Geophys. Res., 70, 4219, 1965.

5. Sonnerup B.U.O. Adiabatic particle orbits in a magnetic null sheet. J. Geophys. Res., 76, 8211, 1971.

6. Stern D.P., Palmadesso P. Drift-Free magnetic geometries n adiabatic motion. J.Geophys. Res., 80, 4244-4248, 1975.

7. Syrovatskii S.I. Pinch sheets and reconnection in astrophysics. Ann. Rev. Astron. Astrophys., 19, 163-229, 1981.

8. Syrovatskii S.I. Formation of current sheets in a plasma with a frozen-in strong magnetic field. Sov. Phys. JETP, 33, 933-940, 1971.

9. Syrovatsky, S.I., On the Appearance of Current Sheet in Plasma with Frozen-in Strong Magnetic Field, Sov. Phys. JETP, 60, 1727, 1971.

10. Chen, J. Nonlinear Dynamics of Charged Particles in the Magnetotail. J. Geophys. Res., 97, 15011-15050, 1992.

11. Coppi, B., G.Laval, R. Pellat Dynamics of the geomagnetic tail, Phys. Rev. Retters, 16, 26, 1207-1210, 1966.

12. Cary, J.R., D.F. Escande, J.L.Tennyson. Adiabatic Iinvariant Change Due to Separatrix Crossing. Phys. Rev. Lett. A, 34, 4256, 1986.

13. Delcourt , D.C., R.F. Martin. Pitch Angle Scattering Near Energy Resonances in the Geomagnetic Tail. J. Geophys. Res., 104, 383, 1999.

14. Wegelmann T., J. Büchner. Kinetic simulations of the coupling between current instabilities and reconnection in thin current sheets. Nonlinear Proc. In Geoph., 7, 141, 2000.

15. Büchner J., Kuska J.-P. Numerical simulation of three-dimensional reconnection due to the instability of collisionless current sheets. Adv. Space Res., 19, 1817, 1997.

C. TEXTBOOKS

1. Introduction to space physics, ed. by M.G.Kivelson, Ch.T.Russel. Cambridge University Press, 1995.

2. Parker E.N. Spontaneous current sheets in magnetic fields. Oxford University Press, 1994.

3. Priest E., T.Forbes. Magnetic reconnection. MHD theory and application. Cambridge University Press, 2000.

4. Somov B.V. Cosmic plasma physics. Kluwer Academic Publishers, 2000.

5. D.Biskamp. Nonlinear magnetohydrodynamics, in Cambridge Monography on Plasma Physics 1, edited by W.Grossman et al.,Cambridge Univ.Press. 1993

6. R.Walker, T.Terasawa, L.Zelenyi, et al. Source and loss processes in the magnetotail. Space Sci.Rev., **88**, 1-2, 285-352, 1999.